RIGA TECHNICAL UNIVERSITY

Aleksandrs Bubovičs

MULTILEVEL CONVERTERS FOR BATTERY INTERFACING

Doctoral Thesis

RTU Press
Riga 2025

RIGA TECHNICAL UNIVERSITY
Faculty of Computer Science, Information Technology and Energy
Institute of Industrial Electronics, Electrical Engineering and Energy

Aleksandrs Bubovičs
Doctoral Student of the Study Programme "Computerised Control of Electrical Technologies"

MULTILEVEL CONVERTERS FOR BATTERY INTERFACING

Summary of the Doctoral Thesis

Scientific supervisor
Professor Dr. sc. ing.
ILYA A. GALKIN

RTU Press
Riga 2025

Bubovičs, A. Multilevel Converters for Battery Interfacing. Summary of the Doctoral Thesis. Riga: RTU Press, 2025. 49 p.

Published in accordance with the decision of the Promotion Council "P-14" of 14 March 2025, Minutes No. 04030-9.12/5.

The Doctoral Thesis was supported by the EU Recovery and Resilience Facility within Project No. 5.2.1.1.i.0/2/24/I/CFLA/003 "Implementation of consolidation and management changes at Riga Technical University, Liepāja University, Rēzekne Academy of Technology, Latvian Maritime Academy and Liepāja Maritime College for the progress towards excellence in higher education, science and innovation" academic career doctoral grant (ID 1015).

Cover picture generated by openAI DALL-E/ChatGPT 4.0.

https://doi.org/10.7250/9789934371752
ISBN 978-9934-37-175-2 (pdf)

DOCTORAL THESIS PROPOSED TO RIGA TECHNICAL UNIVERSITY FOR THE PROMOTION TO THE SCIENTIFIC DEGREE OF DOCTOR OF SCIENCE

To be granted the scientific degree of Doctor of Science (Ph. D.), the present Doctoral Thesis has been submitted for defence at the open meeting of RTU Promotion Council on 30 May 2025, at 14.00 in the Conference Hall of RTU Conference and Sports Centre "Ronīši", Klapkalnciems, Engure County.

OFFICIAL REVIEWERS

Associate Professor Dr. sc. ing. Jānis Zaķis,
Riga Technical University

Associate Professor Ph. D. Carlos Roncero-Clemente,
University of Extremadura, Spain

Senior Lecturer Ph. D. Indrek Roasto,
Tallinn University of Technology, Estonia

DECLARATION OF ACADEMIC INTEGRITY

I hereby declare that the Doctoral Thesis submitted for review to Riga Technical University for the promotion to the scientific degree of Doctor of Science (Ph. D.) is my own. I confirm that this Doctoral Thesis has not been submitted to any other university for the promotion to a scientific degree.

Aleksandrs Bubovičs ……. (signature)
Date: ……

The Doctoral Thesis has been prepared as a thematically united collection of scientific publications. The Doctoral Thesis has been written in English. It consists of an Introduction, five chapters, Conclusions, 49 figures, five tables, and 11 appendices; the total number of pages is 70, not including appendices. The Bibliography contains 104 titles.

CONTENTS

INTRODUCTION

Motivation and background

Nowadays, electrochemical Battery Energy Storages (BES or just batteries) are considered as the most available, reliable and practical storage of electrical energy for a broad range of applications. Batteries are used in such applications as light electrical vehicles, personal mobility vehicles including rehabilitation equipment, portable electronics (for example, laptops, tablets etc.), portable household equipment and handy tools (like vacuum cleaners, robot vacuum cleaners, grass cutting robots, cutting/drilling tools etc.), energy storage systems for power supply needs, as well as in various other applications. The battery interface converter is a necessary part of the configuration. It connects the battery to the load and is needed because even if the voltages of the battery and load are generally comparable, the battery voltage is not constant and depends on various factors, first of all, on State of Charge (SOC) and State of Health (SOH). There also exist AC loads, for example, AC motors/generators and the AC grid. In this case, voltages and currents should be continuously driven as needed by application, having the requested amplitude, frequency, phase of the waveforms and, sometimes, their harmonic content.

The first big group of converters that can link batteries and AC loads includes non-isolated schemes, which in general can be divided into single-stage (efficient only in one operation point) and two-stage converters (with a wider efficient range of operation). In turn, the second big group of battery interfaces includes isolated schemes, which are two-stage by definition. Most of these topologies can serve only as a battery interface, but are not suitable for balancing, which can be considered a disadvantage.

Multilevel converters can be brought forward as the third specific big group of interface schemes, capable of linking batteries and AC loads. The multilevel converters are topologically compatible with batteries that typically consist of several sequentially connected cells. Among all multilevel converter topologies, those with independent sources have one extra advantage of natural (without extra circuits) battery balancing and, therefore, have large potential in applications with batteries. They, however, have certain drawbacks, such as a large number of active and uncontrollable semiconductor switches that increase with the number of levels, leading to higher conduction losses and more complex control. For this reason, finding and implementing classical multilevel topology modifications, which reduce switch count while keeping all the advantages of the topology, would be important. It would improve the parameters of the multilevel converters, extend their use in battery systems and expand the use of these storages.

Main hypothesis and objectives

Hypothesis

Combining an unfolding circuit with a series of independent voltage sources, connected according to a multilevel structure, thus forming a battery interface converter, gives the ability to reduce the switch count and overall losses of the converter, keeping, at the same time, the advantages of the original parts.

Aim and objectives

The aim of the Thesis is to analyze existing multilevel converter topologies and to propose new configurations that are more advantageous in terms of efficiency and control complexity, multilevel battery interface converters, while keeping the advantages of classical multilevel structures. The objectives of the Thesis, therefore, were set as follows:

1. To analyze multilevel converter topologies and their operating principles, in order to identify their disadvantages and outline improvement opportunities.
2. To analyze the topologies of unfolding circuits and their applications.
3. To synthesize battery interface converter(s) as a combination of an unfolding circuit with a multilevel structure with independent sources.
4. To analyze the obtained battery interface converter, made of the above-mentioned parts, applying hybrid (level and pulse width) modulation.

Research methods and tools

The main research method within the Thesis is data collection and analysis. The data are obtained mostly from experiments, partly from mathematical and computer simulations, but sometimes (mostly in the Introduction) from the existing information sources.

MS Excel and *Matlab* have been used for calculations, mathematical modelling, data processing and representation of obtained results. *Matlab-Simulink* was used for modelling and simulations, and *LTspice* was used for preliminary simulations. *Altium Designer* was used as a main tool for PCB design, on rare occasions, *EasyEDA* and *KiCad EDA* were used.

For testing, debugging and experimental verification in laboratory conditions, a variety of laboratory equipment has been used, specially adapted for each experiment that was held: oscilloscopes (*RIGOL DS4012, Tektronix TDS 1024B-EDU*), power supply units (*TTi EX752M, EA-PS 8032-10 T*), thermal camera (*Fluke Ti450*), various multimeters, power analyzer (*PPA5530*). Also, for debugging in certain stages, a digital oscilloscope, a waveform generator, and the logic analyzer *Analog Discovery* was used.

Several microcontrollers from the C2000 family (*F28027 and F28379D*) have been used, as well as the *RP2040* microcontroller. *Code Composer Studio, Pycharm* and *Matlab* plugin for the C2000 microcontroller family were used to program and debug microcontrollers.

Scientific novelty

1. Several new configurations of multilevel converters with independent sources were proposed, including a novel configuration of multilevel converters with independent sources, unfolding circuit and fluent regulation.
2. A method of source balancing within one sine period in multilevel converters with independent sources during discharge has been proposed.
3. A novel system and method for transmitting power between DC and AC sources has been proposed; an application for patent LVP2023000064 was submitted on 12 July 2023.
4. A novel adjustable LED lamp single-inductor multiple-output driver has been proposed; an application for patent LVP2023000103 was submitted on 27 October 2023.

Practical implementation

Research results have been implemented in several national and international research projects:

1. European Regional Development Fund (ERDF) project, within the contract No. 1.1.1.1/16/A/147 “Research and Development of Electrical, Information and Material Technologies for Low Speed Rehabilitation Vehicles for Disabled People”.
2. Baltic Research Program project, funded by the European Economic Area and Norway, 2014–2021, financial mechanisms within the contract EMP474 “Optimised Residential Battery Energy Storage Systems (ORBES)” of the first (Estonian) call of this program.
3. Latvian Council of Science project “Enhanced Thermal Management of Electric Drives in Orthopaedic Rehabilitation Vehicles for their Better Reliability and Functionality”, project No. lzp-2020/2-0390.
4. European Regional Development Fund project in the frame of the contract No. 1.1.1.1/20/A/079 “Research and Development of Two-Phase Thermal Systems Installed in Lighting Equipment for its Functional Improvement” of its Latvian measure 1.1.1.1 “Industry-Driven Research”.

Approbation of research results

In total, the author of the Thesis has 29 publications and two patents. Of them, nine publications, two Latvian patents and two unpublished papers are directly related to the topic of the Doctoral Thesis.

I. I. A. Galkin, A. Blinov, M. Vorobyov, **A. Bubovich,** R. Saltanovs, D. Peftitsis, Interface Converters for Residential Battery Energy Storage Systems: Practices, Difficulties and Prospects. Energies 2021, 14, 3365. https://doi.org/10.3390/en14123365

II. **A. Bubovich**, M. Vorobyov, I. Galkin, A. Blinov, and A. Giannakis, "Overview of Bidirectional Unfolding Converters for Battery Energy Storage Systems," 2022 IEEE

13th International Symposium on Power Electronics for Distributed Generation Systems (PEDG), Kiel, Germany, 2022, pp. 1–7, doi: 10.1109/PEDG54999.2022.9923093.

III. Unpublished paper "Multilevel Unfolding Converter with Independent Sources: Proof of Concept", will be submitted to MDPI Energies by May 2025.

IV. Unpublished paper "Evaluation of Smooth Waveform Regulation in Multilevel Converters with Unfolding Stage", submitted to AIEEE 2025 conference

V. **A. Bubovich**, V. Parinova, I. Galkin, and A. Giannakis, "Initial Evaluation of Multilevel Converter with Unfolding Stage and Voltage Regulators for applications in BESSs," 2022 18th Biennial Baltic Electronics Conference (BEC), Tallinn, Estonia, 2022, pp. 1–5, doi: 10.1109/BEC56180.2022.9935611.

VI. **A. Bubovich**, M. Vorobyov, I. Galkin, and T. Dovudon, "Quality Evaluation of Jointly Used Modular Multilevel Converters and Battery Energy Storages," 2021 International Conference on Electrical Drives & Power Electronics (EDPE), 2021, pp. 144–151, doi: 10.1109/EDPE53134.2021.9604102

VII. **A. Bubovich**, M. Vorobyov, A. Blinov, and D. Peftitsis, "Peculiarities of Multilevel Power Electronic Converters for Interfacing Battery Energy Storages with AC Loads," 2020 IEEE 8th Workshop on Advances in Information, Electronic and Electrical Engineering (AIEEE), 2021, pp. 1–4, doi: 10.1109/AIEEE51419.2021.9435798

VIII. **A. Bubovich**, M. Vorobyov, and A. Giannakis, "Initial Evaluation of a Multilevel Inverter with Unfolding Stage for BESS Applications," 2021 IEEE 9th Workshop on Advances in Information, Electronic and Electrical Engineering (AIEEE), 2021, pp. 1–4, doi: 10.1109/AIEEE54188.2021.9670386.

IX. **A. Bubovich**, I. Galkin, "Evaluation of Optimal Switching of Modular Multilevel Inverter with Independent Voltage Sources". In: 2020 IEEE 61st International Scientific Conference on Power and Electrical Engineering of Riga Technical University (RTUCON 2020): Conference Proceedings, Latvia, Riga, 5–7 November 2020. Piscataway: IEEE, 2020, pp.1–4.

X. O. Tetervenoks, I. Galkin, **A. Bubovich,** Considerations on Practical Implementation of Current Source Mode Single-Inductor Multiple-Output LED Driver. Electronics 2024, 13, 54. https://doi.org/10.3390/electronics13010054

XI. I. A. Galkin, R. Saltanovs, **A**. **Bubovich,** A. Blinov, D. Peftitsis, Considerations on Combining Unfolding Inverters with Partial Power Regulators in Battery–Grid Interface Converters. Energies 2024, 17, 893. https://doi.org/10.3390/en17040893

XII. R. Saltanovs, I. Galkins, **A. Bubovičs**, A. Blinov, D. Peftitsis, SYSTEM AND METHOD FOR TRANSMITTING POWER BETWEEN DC AND AC SOURCES. Latvian patent application LVP2023000064, Patent application date 12.07.2023.

XIII. O. Tetervenoks, I. Galkins, **A. Bubovičs**, Adjustable LED Lamp Single Inductor Multiple Output Driver. Latvian patent application LVP2023000103, Patent application date 27.10.2023.

Publications related to the Doctoral Thesis, which were not included in the summary of the Doctoral Thesis:

1. **A. Bubovich**, I. Galkin, "Evaluation of Multilevel Inverter with Unfolding Stage and Voltage Regulators for BESS Applications". In: Proceedings of the 21st International Symposium "Topical Problems in the Field of Electrical and Power Engineering" and "Doctoral School of Energy and Geotechnology III", Estonia, Pärnu, 15–18 June 2022. Tallinn: TalTech, 2022, pp. 57–58. ISBN 978-9949-83-859-2
2. **A. Bubovich**, "Use of Multilevel Converters in Light Vehicles of Orthopedic Rehabilitation," 2021 IEEE 62nd International Scientific Conference on Power and Electrical Engineering of Riga Technical University (RTUCON), 2021, pp. 1–4, doi: 10.1109/RTUCON53541.2021.9711728
3. **A. Bubovich**, "Evaluation of Opportunities of Balanced Discharge of Batteries in Cost Effective Assisting Powered Wheelchair". In: Proceedings of the 19th International Symposium "Topical Problems in the Field of Electrical and Power Engineering" and "Doctoral School of Energy and Geotechnology III", Estonia, Tartu, 14–17 January 2020. Tallinn: TalTech, 2020, pp. 135–136. ISBN 978-9949-83-518-8
4. **A. Bubovich**, "Evaluation of opportunities of balanced discharge of batteries in cost effective assisting powered wheelchair", 2019 IEEE 60th International Scientific Conference on Power and Electrical Engineering of Riga Technical University (RTUCON 2019), Riga, 2019.

ABBREVIATIONS

ADC	Analog-to-Digital Converter
AEV	All-Electric Vehicles
BES	Battery Energy Storage
BESS	Battery Energy Storage System
CCS	Constant Current Source
CR	Current Regulator
CSM	Current Source Mode
DAB	Dual Active Bridge
EMC	Electromagnetic Compatibility
FET	Field Effect Transistor
HFHD	High Frequency Harmonic Distortion
IC	Integrated Circuit
LA	Lead-Acid *(battery technology)*
LED	Light Emitting Diode
LFHD	Low Frequency Harmonic Distortion
LR	Light flux Regulator
MCU	Microcontroller Unit
MDS	Maximal Duration of Switching
MLC	Multilevel Converter
MOSFET	Metal Oxide Semiconductor Field Effect Transistor
PEV	Plug-in Electric Vehicle
PFC	Power Factor Correction
PV	Photovoltaic
PWM	Pulse Width Modulation
RFB	Redox Flow Battery
RGB	Red, Green and Blue *(additive color model)*
SEPIC	Single-Ended Primary Inductor Converter
SIMO	Single Inductor Multiple Output
SLLS	Segmented LED Light Source
SOC	State of Charge
SOH	State of Health
THD	Total Harmonic Distortion
UF	Unfolding Frontend
VSI	Voltage Source Inverter
VRB	Vanadium Redox Battery
ZCS	Zero Current Switching
ZVS	Zero Voltage Switching

1. APPLICATION OF BATTERIES IN MODERN TECHNOLOGIES

Author's Publications I [1] and II [2] are related to Chapter 1.

1.1. Development of electrochemical energy storages

The most intensive development of electrochemical energy storage systems has taken place since the late 20th century and is still progressing. The demand for portable electrical devices, vehicular technologies and energy systems is constantly growing, and because of that, technologies of already known battery electrochemistries have been "polished" and new battery technologies have been introduced into the market. Nowadays, the most significant battery technologies are advanced lead-acid (LA), nickel-oxyhydroxide (NiMH), sodium-sulfur (NaS), various kinds of Li-ion batteries, as well as redox flow batteries (RFBs), in particular, vanadium redox batteries (VRBs) [3], [4].

LA technology, the oldest among others, is the cheapest and also has quite high efficiency. However, the main drawbacks of this technology are that LA batteries have rather low specific energy and comparably low charge-discharge cycles (i.e. lifetime). Historically, the next successive NiMH technology (replacement for NiCd) is characterized by average specific power and has a low charge-discharge efficiency (approximately 65 %). The NaS batteries have quite high specific energy, energy efficiency and lifetime (90 % and 4000 cycles, respectively [4]). However, the main drawback of NaS batteries is quite high operation temperature, which means that they require heating. This fact makes the application of these batteries impractical in many cases. Nowadays, the fastest-developing battery technology is the Li-Ion. Li-Ion batteries have high specific energy, specific power, lifetime (up to 10,000 cycles), energy efficiency (up to 95 %), achieved at a reasonable price, making the technology very applicable in portable electronics, all-electric vehicles, household energy systems and even in energy distribution grids [5]. However, specific parameters of Li-Ion batteries depend on the corresponding chemistry, and all advantages are typically not concentrated in one device. Finally, RFBs, in particular VRBs, are the batteries that utilize a reduction-oxidation reaction between two liquids, which occurs through a membrane. The liquids are pumped to the membrane, which makes RFBs similar to fuel cells, where the liquids are chemically restorable. The main advantage of these batteries is their potentially infinite lifetime. Lastly, it must be mentioned that modern batteries are not just a series connection of galvanic cells. They often include electronics for balancing, management and protection, as well as chargers in some cases. Therefore, these batteries can be considered as complex complete energy units for immediate use [6]–[8]. Figure 1.1 shows the comparison between different commercially available batteries.

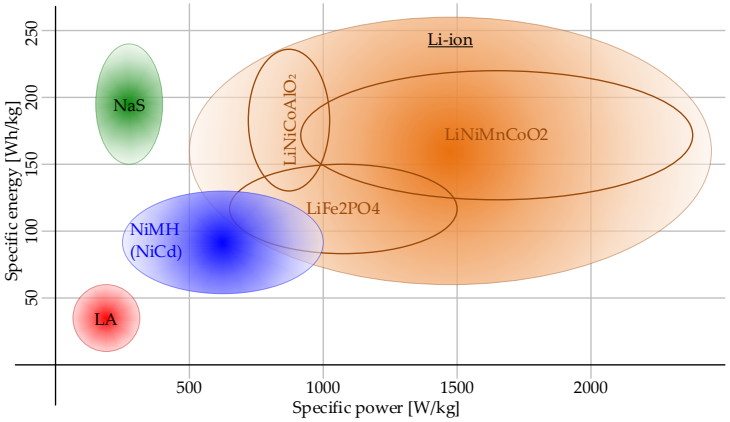

Fig. 1.1. Specific energy and specific power of the commercially available batteries.

1.2. Motivation for use of batteries

With the development of electronic technologies, portable electronic devices have been rapidly growing over the past decades. The primary motivation of this growth is that portable electronic appliances are widely used in our daily life, from low power appliances, for example, flashlights, TV remote controls, scales, watches, to more power-consuming devices, for example, laptops, tablets, robot vacuum cleaners, etc.

Application of batteries in transport

One of the recent global societal and legislative tendencies on the national and international levels is the request to reduce the consumption of fossil fuels and to increase the efficiency of energy consumption [9], [10]. Among other areas, this involves vehicular technologies as well. Regarding ground vehicles, this initiative means wider use of plug-in electric vehicles (PEVs) or all-electric vehicles (AEVs) and hybrid ones, equally in the public and private sectors. In [11], [12], the availability of cost-effective batteries of several hundred volts for the main electrochemical energy storage of PEV is reported. Papers [13]–[16] consider these PEV storage systems valuable enough to be a part of the energy supply grid. Further development of the BESs makes their use possible in larger ground vehicles, first of all, in public transport [17], [18].

Better BESs are also required for water vehicles, first of all, for smaller auxiliary vehicles – boats, yachts, water buses, etc. For example, in [19], the electrification of the water buses in Venice is considered a successful example of BES use in water transport. At the same time, with regard to bigger ships and vessels, the role of BESs differs with time. While earlier configurations of marine energy systems utilize high voltage batteries for stabilizing the traditional onboard AC grid and power smoothing [20], [21], modern systems also take into account the possibility of all-electric propulsion of the ship [21], [22].

Application of batteries in power and energy supply

The request to reduce fossil fuel consumption [9], [10] regards also power distribution and supply networks. For the power and energy supply systems, this means that the burning of fossil fuels must be substituted with renewable energy generation. In turn, the main properties of renewable energy generation are as follows:

- Uneven generation profile – regardless of the kind, the renewable energy sources typically do not provide constant power. In particular, the generation of PV panels depends on solar irradiation and varies with the daytime, cloudiness, season, location of PV and solar activity. The generation of wind turbines depends on the wind strength, which is unique for its location, season and occasional weather fluctuation. The generation of hydro and wave turbines depends on the amount of water, which is a long-term function of seasonal and global weather changes.
- A variety of power ratings and types of energy sources exist even within the same group. For example, the power of PV depends on the local properties and financial abilities of a particular household.
- Variety of allocation of the renewable energy sources – depending on the particular economic conditions and policy of the energy operator, these sources may be allocated differently.

Altogether, this makes renewable energy generation less stable and reliable. This, as well as several other problems [23]–[28], can be solved with the help of Battery Energy Storage Systems (BESSs). In the distribution grids, the functions of the dedicated BESS are similar but more specified. Price compensation now can be considered as a complete function of energy trading, smoothening of power generation regards not only renewables, but smoothening of consumed power at this level saves the capacity of distribution equipment. Additionally, BESS in distribution grids may perform grid service functions: grid black restart, as well as voltage and frequency regulation [24], [29]. The choice of BESS parameters is a subject of multiple factors [30]: standards, power losses, voltage of the majority of available PEVs, compatibility with pure resistive loads.

1.3. Configurations of battery interface converters

In all applications, described in Section 1.2, the battery interface converter is an essential part. The choice of the converter topology is mainly dependent on the configuration of the battery and the load. Figure 1.2 shows possible configurations of batteries and loads.

Considering the configuration of the battery and load, the topology of the interface converter should be chosen. Taking into account that, especially with application in power and energy supply, the battery should not only be charged but also discharged, it is reasonable to narrow the variety of battery interface converters to bidirectional ones.

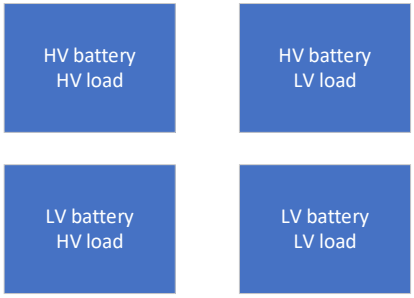

Fig. 1.2. Possible configurations of batteries and loads.

If the voltage of the battery and the load are close to each other, a non-isolated topology can be chosen. However, the main disadvantage of this type of converter is that it operates at maximal efficiency only at one point. Also, there are single-stage converters and two-stage converters. Two-stage converters allow for increasing the efficient operation range of non-isolated converters. If the battery and load have different voltage ratings, then isolated topologies can be chosen. An example of such a topology is Dual Active Bridge (DAB). Table 1.1 represents bidirectional converters with examples, characteristics of BES and peculiarities.

Table 1.1

Bidirectional Battery Interface Converters

Bidirectional converter		**Characteristics of BES**	**Peculiarities**
Non-isolated topologies	Non-inverting buck-boost converter	Low voltage Low to medium power	Easier voltage regulation. Higher maximal efficiency, but a small range of higher efficiency.
	Ćuk, SEPIC, Zeta	Low voltage Low power	
Isolated topologies	DAB converter	Low to medium voltage Low to medium power	Soft switching capability. Galvanic isolation.
Multilevel topologies	Multilevel converter with independent sources	Low to high voltage Low to high power	Natural battery balancing capability. Sophisticated control.

2. ANALYSIS OF MULTILEVEL CONVERTER CLASSICAL TOPOLOGIES

Author's publications I [1], VII [31] and IX [32] are related to Chapter 2.

Multilevel converters (MLC) can be considered as a specific kind of single-stage inverters, processing energy in separate cells of a battery. In contrast to the topologies mentioned in Section 1.3, which always deal with the same DC voltage or with the entire battery, MLCs form their output of DC voltage that may have several levels, obtained directly from the battery. The advantages of multilevel converters are lower harmonic distortion, switching losses and electromagnetic interference [33]. There are three main topologies of MLCs: neutral point clamped multilevel converter (also known as diode clamped multilevel converter), multilevel converter with flying capacitors and multilevel converters with independent sources.

Output waveforms of MLCs can be either level-modulated (output waveforms are stepped and formed only by adding/removing voltage levels to the output waveform) or PWM modulated.

In the literature, there are multiple versions of the term *level* definition in MLCs. There is a version where all possible voltage levels are taken into account (positive, negative and 0 V). Another version of the term *level* is when only positive voltage levels and 0 V are considered. Hereinafter, the term *level* implies all positive voltage levels, not including 0 V.

The output phase voltage waveform in the case of level modulation for one phase cascade with s levels can be described with the help of the Fourier transform:

$$V(\omega t) = \frac{4V_g}{\pi} \sum_n [\cos(n\alpha_1) + \cos(n\alpha_2) + ... + \cos(n\alpha_s)] \cdot \frac{\sin(n\omega t)}{n}, \tag{2.1}$$

where

V_g – source input voltage;

ω – angular frequency;

$\alpha_1, \alpha_2, ..., \alpha_s$ – level conducting angles.

Level conducting angles can be chosen in such a way that total harmonic distortion is minimal. If sinewave with phase angle φ equal to 0 radians, amplitude is equal to 1 V and frequency $f = 1$ Hz is examined as reference signal for single level voltage source inverter (VSI), or simply full transistor bridge, and instead of radians on x-axis of a plot time in seconds is taken (see Fig. 2.1 (a)), then instead of conducting angle θ there is conducting time t_{sw}. Considering that a sinewave is symmetrical, only one quarter of the sinewave should be examined. As shown in Fig. 2.1 (a), during time period from 0 to $T/4$, there is one commutation time (or level switching time), in Fig. 2.1 (a), it is denominated as t_{sw}. If a line $t = t_{sw}$ is drawn, then there are two areas: $S1$ and $S2$, that show the displacement of the generated output voltage by a 3-level multilevel inverter with independent sources from the reference sinewave. Areas $S1$ and $S2$ can be calculated by Equations (2.2) and (2.3):

$$S_1 = \iint_{S_1} dtdV = \int_0^{t_x} dt \int_0^{\sin(\omega t)} dV \tag{2.2}$$

$$S_2 = \iint_{S_2} dtdV = \int_{t_x}^{T/4} dt \int_{\sin(\omega t)}^{1} dV \tag{2.3}$$

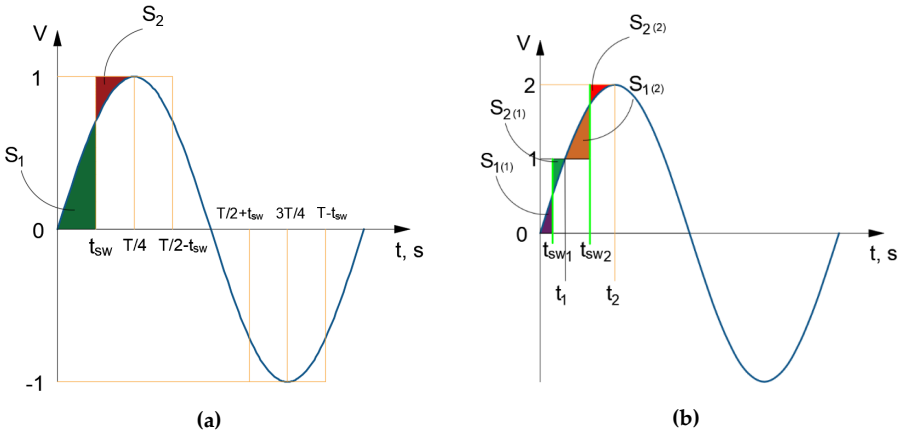

Fig. 2.1. Reference sinewave for (a) VSI; (b) 2-level MLC.

In order to have minimal THD, the sum of areas S_1 + S_2 should be minimal, and the only parameter that can be changed in this case to make changes in S_1 and S_2 is the switching time. The same principles of calculation are applicable when the level count is different (2, 3, 4, 5, etc.); the only thing that changes is the borders of the y-axis. It is convenient to use a reference sinewave with amplitude 2 for 2-level MLC, with amplitude 3 for 3-level MLC, etc. In Fig. 2.1 (b), the reference signal for the 2-level multilevel inverter is shown.

2.1. Neutral point clamped multilevel converters

Neutral point clamped MLCs were first introduced in 1981 by A. Nabae, I. Takashi, and H. Akagi [34]. To separate the DC voltage into different levels, capacitors are used. The voltage across each switch is limited to the voltage of a capacitor by means of the diode. The main advantage of this topology is quite high efficiency compared to other topologies. However, there are some disadvantages: the number of power diodes is quadratically related to the level count, which makes this topology quite difficult to use when a large number of levels is needed [35]. Another disadvantage of the topology is that charge balancing in capacitors is needed. Figure 2.2 (a) shows diode neutral point clamped multilevel converter. The use of neutral point clamped converters in the energy storage system is described in [36]. Paper [37] describes the use of a neutral point clamped converter in the AC part of the BESS grid-connected system.

The neutral point clamped multilevel converter has one subtype – active neutral point clamped multilevel converter, shown in Fig. 2.2 (b). The main advantage of this topology – additional switches – gives the ability to distribute power losses more evenly between switches. Also, it is possible to provide a 0 V level by different paths. Paper [38] shows the use of neutral point clamped and active neutral point clamped converters in battery energy storage systems.

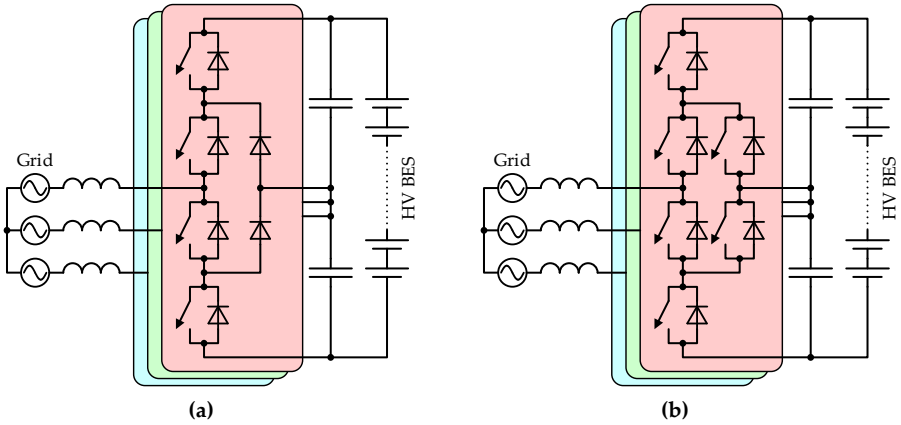

Fig. 2.2. Neutral point clamped MLCs: (a) three-phase diode clamped MLC; (b) three-phase active neutral point clamped MLC.

2.2. Multilevel converters with flying capacitors

MLC with flying capacitors was introduced by Thierry A. Meynard and Henri Foch in 1992 [39]. The main difference between neutral point clamped MLC and MLC with flying capacitors is that instead of clamping diodes, capacitors are used, forming a ladder structure, where the voltage of one capacitor leg is different from that of the other capacitor leg for one phase. Figure 2.3 shows the MLC with flying capacitors.

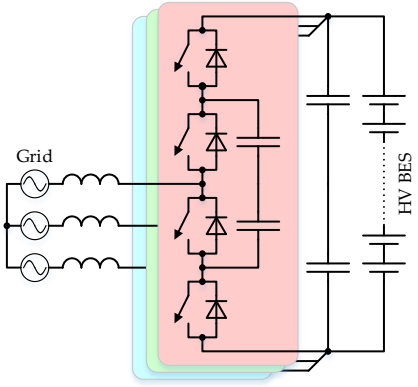

Fig. 2.3. Three-phase flying capacitor MLC.

This topology has one advantage – if a number of levels allows that, the necessary amplitude output voltage can be synthesized with multiple switch combinations. Similar to the diode-clamped topology, the main disadvantage of the MLC with flying capacitors is the large number of used capacitors, which makes the practical implementation of this solution larger in terms of packaging.

2.3. Multilevel converters with independent sources

In case of MLCs with independent sources, one phase cascade consists of several single-phase full bridge converters connected in series; the inputs for full bridge converters are separate (independent) DC sources [40]. Considering that DC sources are independent, this makes this topology advantageous in terms of using it with batteries. DC sources can be charged and discharged more evenly – DC sources are separate and can be turned on and off independently. This fact makes this classical MLC topology more advantageous than the others – battery balancing in this case can be performed naturally. An additional advantage of topology is the modular implementation, which makes the manufacturing process of the converter cheaper.

Figure 2.4 shows a structural schematic of a three-phase MLC with independent sources. Each transistor H-bridge can generate three output voltages: + V_g (switches Q1 and Q4 are turned on), 0 V (switches Q1 and Q2 or Q3 and Q4 are turned on) and – V_g (switches Q2 and Q3 are turned on).

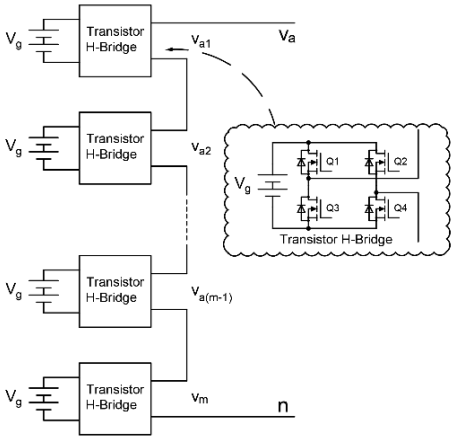

Fig. 2.4. Single-phase MLC with independent sources.

As was previously mentioned, the main advantage of the topology is the ability of independent operation of series-connected sub-modules, which allows for balancing batteries used as sub-module sources.

The State of Charge (SOC) of a battery can be expressed as a percentage of the remaining capacity of the battery (the available or "real" capacity) of the maximal (initial) capacity of a battery [41]:

$$SOC = \frac{\text{Real capacity}}{\text{Initial capacity}} \tag{2.4}$$

If submodules operate without source balancing, and sources are connected to the output depending on the position, then activation of modules will look like it is shown in Fig. 2.5 (a).

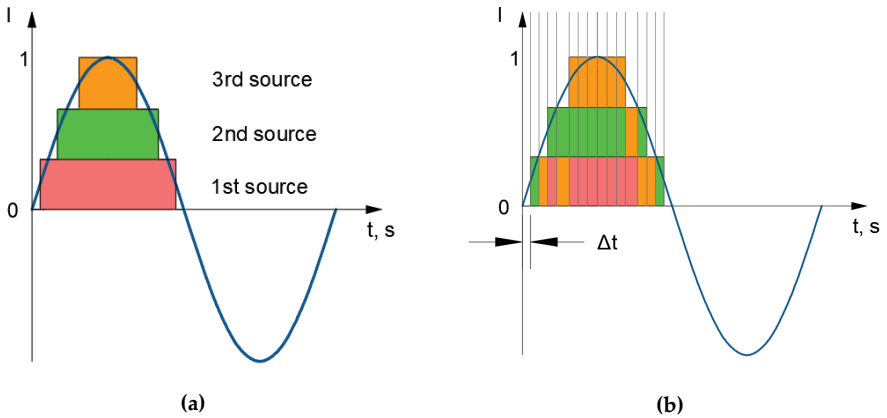

Fig. 2.5. Current waveform formation of MLC with independent sources: (a) unbalanced; (b) with proposed balancing algorithm.

If sub-modules are operated in such a way, it will cause uneven discharge of sources. To improve the discharge, a balancing algorithm of MLC with independent sources was proposed.

In case of three-phase MLC with independent sources, let the SOC_a, SOC_b and SOC_c be the mean value of the state of charge of all batteries connected as sources to H-bridges of one phase cascade (a, b and c phases respectively). For m-level MLC with independent sources, these can be defined as:

$$\begin{aligned} SOC_a &= \frac{1}{m}\sum_{i=1}^{m} SOC_{a,i} \\ SOC_b &= \frac{1}{m}\sum_{i=1}^{m} SOC_{b,i} \\ SOC_c &= \frac{1}{m}\sum_{i=1}^{m} SOC_{c,i} \end{aligned} \tag{2.5}$$

If the time is divided by periods of time Δt, then for each Δt consumed, the amount of charge can be calculated for each battery by multiplying the current by the Δt, and, therefore, the matrix with the real state of charge of the batteries can be calculated. The example of a 3-level MLC with independent sources will look like this:

$$SOC = \begin{pmatrix} SOC_{a1} & SOC_{b1} & SOC_{c1} \\ SOC_{a2} & SOC_{b2} & SOC_{c2} \\ SOC_{a3} & SOC_{b3} & SOC_{c3} \end{pmatrix}. \tag{2.6}$$

If in one period for each Δt the SOC of all batteries is calculated, then turned on batteries can be swapped in such a manner that batteries with larger SOC are utilized more frequently, as is shown in Figure 2.5 (b). During each period Δt, matrix of differences between real values of SOC and the mean values of SOC for each phase ΔSOC should be calculated:

$$\Delta SOC = \begin{pmatrix} SOC_a - SOC_{a1} & SOC_b - SOC_{b1} & SOC_c - SOC_{c1} \\ SOC_a - SOC_{a2} & SOC_b - SOC_{b2} & SOC_c - SOC_{c2} \\ SOC_a - SOC_{a3} & SOC_b - SOC_{b3} & SOC_c - SOC_{c3} \end{pmatrix}. \quad (2.7)$$

ΔSOC should be kept minimal, which would result in submodule "swapping", and such estimation is performed during each Δt. For evaluation, a *Matlab-Simulink* model of a 3-level MLC with independent sources was developed (see Fig. 2.6).

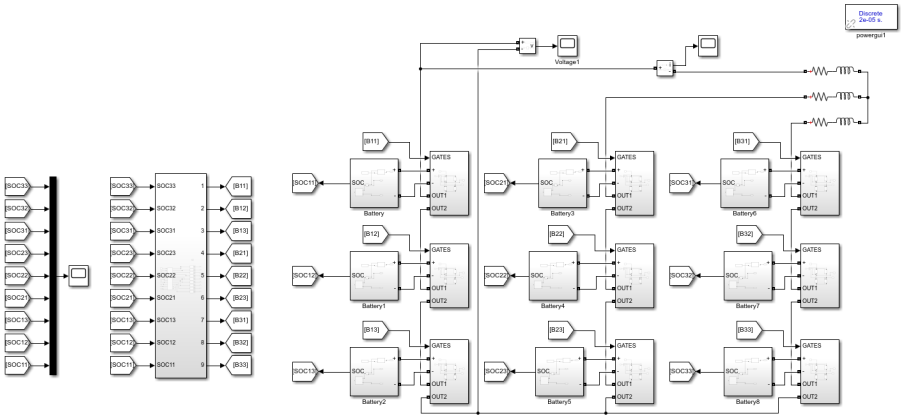

Fig. 2.6. Simulink model of 3-level MLC with independent sources.

Evaluation results are shown in Fig. 2.7. Without a balancing algorithm, batteries are discharged unevenly, which is shown in Fig. 2.7 (a). In turn, when the algorithm is implemented, SOC waveforms form one straight line, which means that batteries are discharged evenly, which is shown in Fig. 2.7 (b).

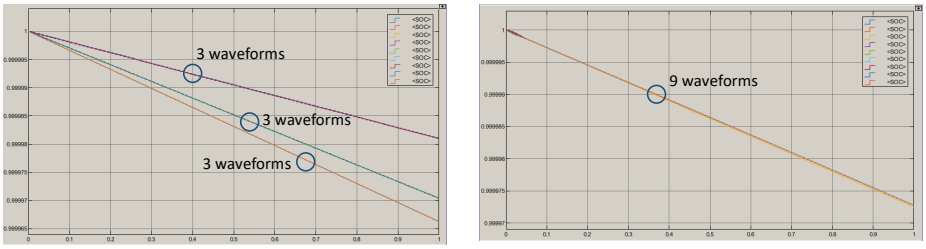

(a) (b)

Fig. 2.7. SOC of batteries of 3-level MLC with independent sources: (a) unbalanced; (b) with balancing algorithm.

3. ANALYSIS OF UNFOLDING CIRCUIT APPLICATION IN POWER ELECTRONIC CONVERTERS

Author's publications II [2] and XI [42] and patent XII are related to Chapter 3.

Considering the application of converters in power and energy supply and with AC loads, an inverter (DC-AC converter) should be used. Speaking about two-stage inverters, there are two alternatives for DC-AC stage operation. Figure 3.1 shows these two alternatives.

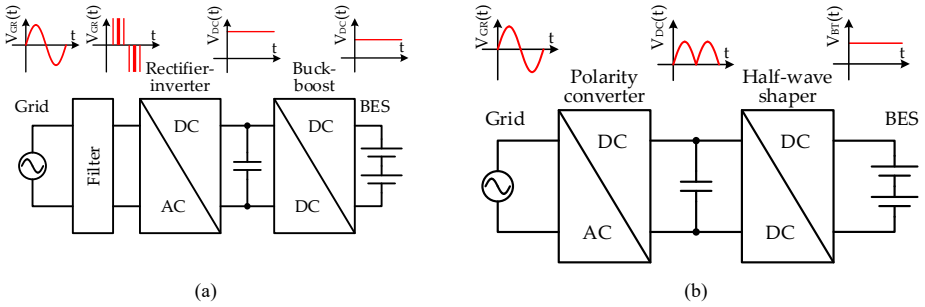

Fig. 3.1. Single-phase MLC with independent sources.

Figure 3.1 (a) shows the case when the AC-DC stage (frontend) operates in pulse mode, modulating the grid voltage according to the phase of the grid voltage and the required grid current, while the DC-DC stage provides a stabilized voltage in the DC-link at all operation points of the battery. This case also has another advantage – stable DC-link voltage allows integration of other DC sources and loads.

Figure 3.1 (b) shows a different operation mode of the frontend. In this case, the DC-DC stage forms unipolar sine half-waves in the DC-link (forming so-called *virtual* or *quasi-DC-link*), and the frontend applies formed half-waves to the grid with the correct polarity. In this case, the frontend does not operate in a real switch-mode, but commutates half-waves at grid frequency. This commutator is called an *unfolding circuit* (or simply *unfolder*).

Application of the unfolding circuit as a part of a two-stage converter gives the ability to reduce the overall losses of the converter. It is known that the largest source of losses of a transistor is the commutation losses. If an unfolding circuit is applied, then commutation losses of the frontend are minimal and in some cases can even be neglected.

The unfolding frontend is composed of a commutation matrix, switching at grid frequency, and an inductance coil that serves as a current forming element and which can be allocated at the DC or AC port of the frontend. Figure 3.2 shows both options of unfolding frontend.

When the coil is allocated at the AC port (as shown in Fig. 3.2 (a)), the first contact of the coil is fixed at the grid, while the second contact is connected through the commutation matrix to the DC-link. Then the coil operates with alternating sine current and voltage. Since the voltage in the grid must be in line with the grid current formed in the coil, the voltage in the coil must have a +/–90° shift. Therefore, the voltage at the first end of the coil (at the AC port of the commutation matrix) must be slightly leading for battery loading mode, or lagging for battery charging mode and slightly higher, compared with the grid voltage on the second end

of the coil. This means that the commutation matrix must be a four-quadrant converter, capable of conducting current in both directions at both polarities of the voltage.

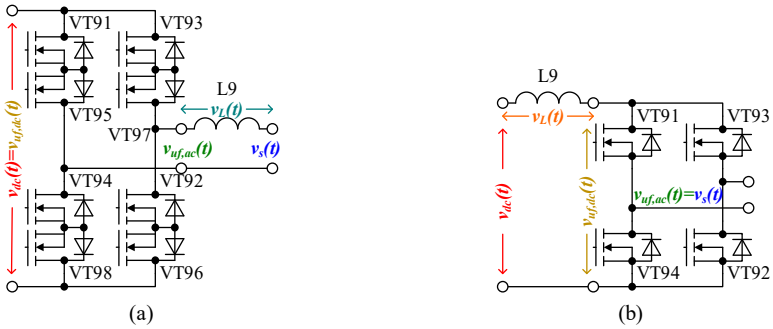

Fig. 3.2. Configurations of unfolding frontend: (a) with current forming coil at AC port; (b) with current forming coil at DC port.

Alternative allocation of the current limiting and forming inductance coil is at the the DC port of the commutation matrix. Then, the first end of the coil is attached to the DC-link voltage, but at the second end, the matrix forms a semi-sinusoidal grid voltage. Then the voltage over the coil is semi-sinusoidal with a 90° shift. With such a configuration, the polarity of the voltage at the AC port of the frontend always corresponds to the polarity of the current. Therefore, the commutation matrix may be a common transistor H-bridge, shown in Figure 3.2 (b).

3.1. Non-isolated topologies

A number of DC-DC choppers for two-stage converters with unfolding circuit exist. The major part deals with unidirectional applications like photovoltaic (PV) systems. However, the review of these systems is important for further understanding of the operation of bi-directional choppers.

Papers [43], [44], and [45] propose buck-boost choppers in grid-connected PV systems. The combination of buck and boost operation modes, combined with an unfolding circuit, gives the ability to regulate the voltage to match the value of the grid voltage.

Paper [46] shows the simulation of model predictive control of the buck-boost converter with the unfolding circuit. Papers [47] and [48] also describe the application of UCs in PV systems. In [47], the combination of buck converter and unfolding circuit is implemented in the form of a low-profile microinverter. Paper [48] focuses on the high-gain operation of the boost converter, tied with a full-bridge unfolding circuit. In addition, this unfolding circuit is working in partial sine-form PWM when the voltage has to be stepped down.

An example of buck-boost topology with integrated unfolding circuit (Aalborg inverter) is described in [49], [50], and [51]. Paper [52] describes the implementation of an isolated Ćuk converter with an unfolding circuit as a differential power processor for aircraft applications. In this case, the unfolding circuit gives the ability of four-quadrant operation of the converter and reduces the worst-case processed power. Paper [53] describes the evaluation of inverter topology based on a buck converter and unfolding circuit within Google's "Little Box

Challenge". The major advantage of the topology is the reduction of volume and complexity of the system. Figure 3.3 shows three configurations of non-isolated topologies with an unfolding frontend.

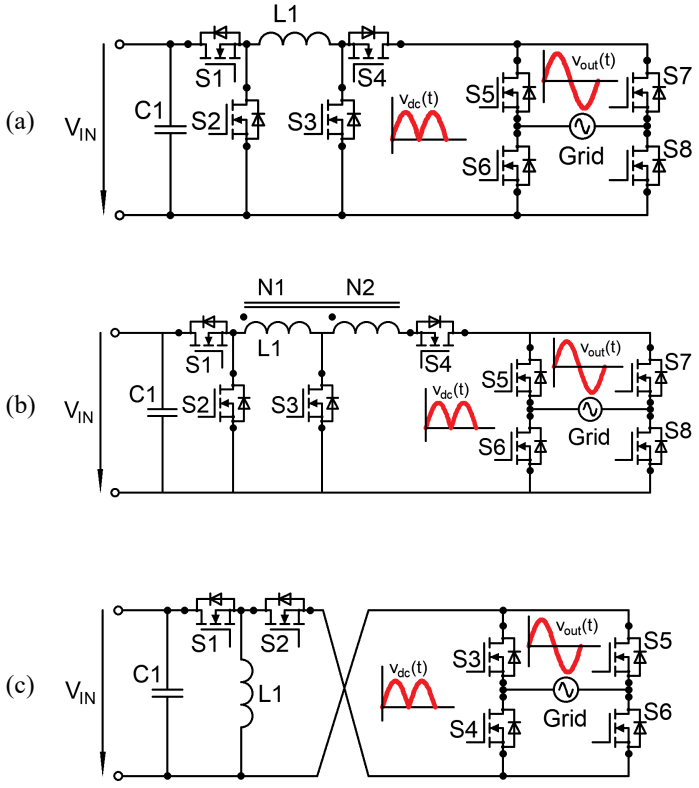

Fig. 3.3. Non-isolated topologies with unfolding circuits: (a) single inductor buck-boost converter with unfolding circuit; (b) tapped inductor buck-boost converter with unfolding circuit; (c) single inductor twisted buck-boost converter with unfolding circuit.

3.2. Isolated topologies

A particular configuration is based on a dual active bridge (DAB). Typically, the DAB is connected with a power factor correction (PFC) rectifier through an intermediate DC link. DAB gives the ability of bidirectional energy flow, which perfectly fits the requirements of BESS [54], [55].

Most commonly, DAB contains two full bridges, a series inductor and a high frequency (HF) isolation transformer (Fig. 3.4) [54]–[62]. The main advantage of the DAB topology is easy implementable zero-voltage switching (ZVS), which decreases the power losses of the converter.

There are two main types of DAB converters: current-fed and voltage-fed. The voltage-fed DAB converters are implemented in various applications, where bidirectional power flow is needed. One of the simplest control methods of the voltage-fed DAB converters is phase shift control [63]–[65]. With phase shift control, both H-bridges of DAB operate with the same duty cycle. In this case, power is controlled by the phase shift between the sides of the DAB converter [66]. Combining the phase shift with PWM enables minimizing the losses of the converter and also extends the operation range, when ZVS can be provided [67], [68]. Papers [69] and [70] describe a series resonant DAB converter. An LC circuit is added at the primary side of the transformer to provide series resonance. By adding a series resonant circuit to the topology, it is possible to achieve ZCS (zero current switching) operation of the DAB converter. Figure 3.4 shows three of the above-described configurations of the DAB converter.

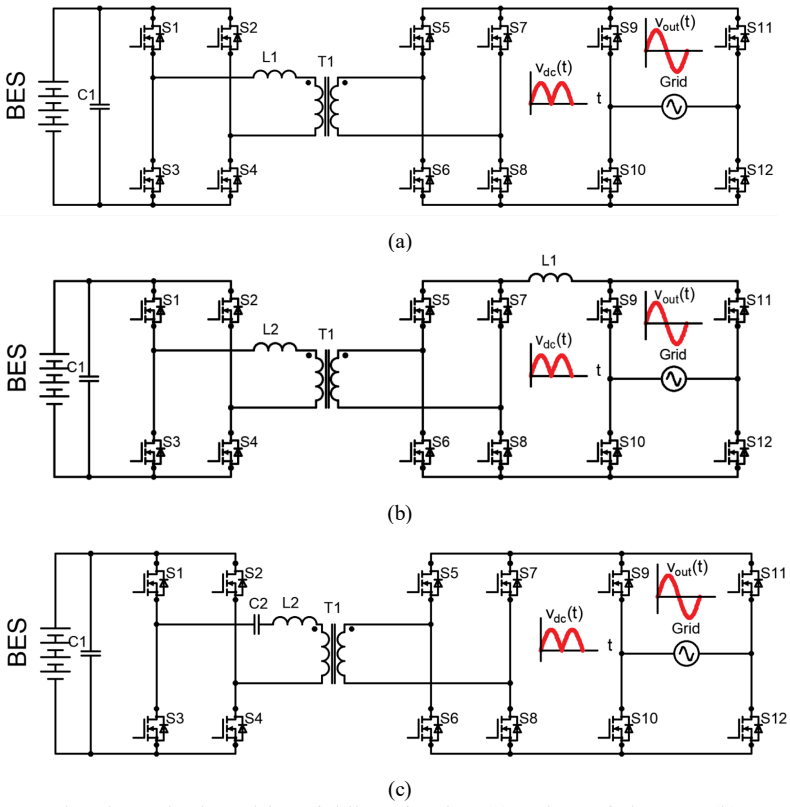

Fig. 3.4. Isolated topologies with unfolding circuits: (a) voltage-fed DAB; (b) current-fed DAB; (c) series resonant DAB.

4. UNFOLDING MULTILEVEL CONVERTERS WITH INDEPENDENT SOURCES

Author's publications II [2], VIII [71] and the unpublished paper III are related to Chapter 4.

Unfolding frontend can also be combined with multilevel half-sine shapers. Classical configuration of MLC with independent sources without an unfolder assumes that several H-bridge modules, fed from a small group of battery cells, are connected in series, thus creating one phase cascade [72]. The use of MLCs in BESS provides natural balancing of battery cells without an explicit battery management system.

Adding an unfolding circuit at the grid side enables bipolar operation of the MLC shaper [71]. It turns the series-connected H-bridges into half bridges, because the bipolar operation of these modules is not necessary. Figure 4.1 shows the configuration of the one-phase cascade with and without the unfolding circuit. Therefore, the use of an unfolding circuit reduces switch count in current paths and, therefore, simplifies the design.

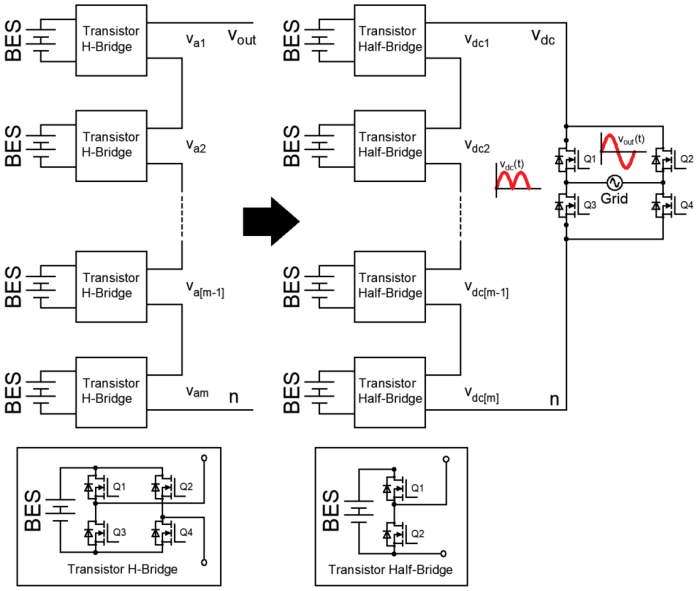

Fig. 4.1. Structure of MLC with and without unfolding frontend.

4.1. Evaluation of operation

To evaluate the performance of MLC with independent sources and an unfolding frontend, a testbench of a 3-level MLC with an unfolder was developed. IRF540 n-channel MOSFETs have been utilized for the switches' realization due to their relatively low cost and high reliability. HCPL-3120 optocouplers were chosen for driving the MOSFETs with bipolar voltage modulation: +15 V for logical "1" and –15 V for logical "0". In order to operate the MOSFETs with this voltage scheme, each HCPL-3120 is connected to the IR0515S board mount power supply with an input voltage equal to 5 V. The LAUNCHXL-F2837D

development board from Texas Instruments has been used to control the operation of the converter. Input voltage was set equal to 8.4 V, which equals the voltage of two fully charged series-connected 18650 battery cells. The developed testbench is shown in Fig. 4.2. An RL load was utilized for the performance evaluation (R = 16 Ω and L = 5 mH).

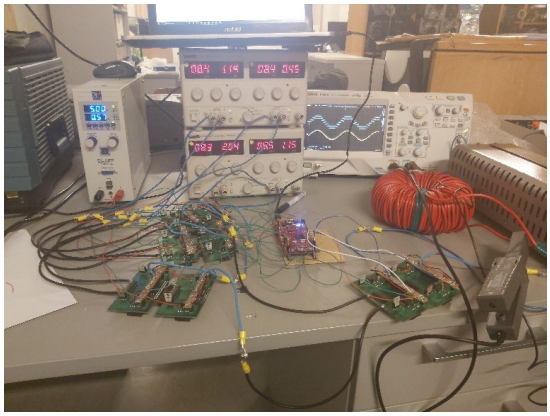

Fig. 4.2. Testbench of MLC with independent sources and unfolding frontend.

Evaluation results are shown in Fig. 4.3.

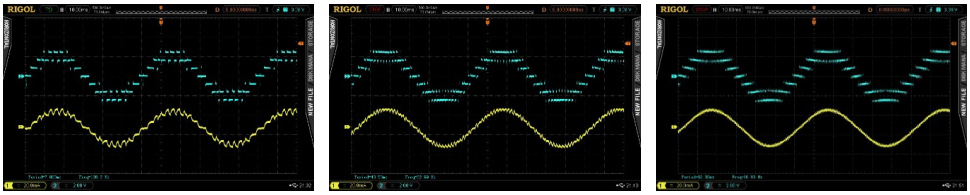

(a) (b) (c)

Fig. 4.3. MLC with unfolder evaluation results (blue waveform – voltage, yellow – current): (a) 1 kHz PWM modulation frequency; (b) 2 kHz PWM modulation frequency; (c) 3 kHz PWM modulation frequency.

The experimental results reveal the proper operation of the MLC with independent sources and the unfolding circuit. The impact of the switching frequency of the converter on the distortion of the output current can be observed. In particular, at 1 kHz switching frequency, the pulsations of the output current are significantly larger compared to the corresponding waveform at 4 kHz.

4.2. Evaluation of the impact of unfolding the frontend on power losses

The influence of combining an unfolding circuit with MLC with independent sources is studied in this section. It is based on the mathematical models of MLC with independent sources, with and without an additional unfolding circuit. In the case of classical MLC with independent sources, the output current of series-connected H-bridge converters is sinusoidal. The output voltage of each H-bridge is equal to $+V_{bat}$, 0 V and $-V_{bat}$ (V_{bat} being source voltage,

typically battery in BESS applications), and the output voltage of the cascade is equal to the sum of the output voltages of each transistor H-bridge. When the unfolding circuit is applied, series-connected H-bridges are conducting semi-sine current. As for the commutated voltage, each half-bridge commutates the voltage of the input battery. The cascade of series-connected transistor half-bridges generates unipolar voltages that are applied to the grid by means of the unfolding circuit with a correct polarity.

Previously, it was mentioned that the combination of an unfolding inverter with MLC gives the ability to reduce the loss of MLC with independent sources. For a simplified analysis of the converter losses, several assumptions should be made:

- Commutated voltages of series-connected sub-modules are equal to the fractions of peak grid voltage equally distributed between sources (i.e., for example, for a 3-level converter source (battery) voltage $V_{bat} = 325/3 \approx 108.33$ V).
- Voltage rise time and voltage fall time of the MOSFET transistor are equal and are proportional to commutated voltage (i.e., they are the same for constant voltage and the same number of levels).
- Current rise time and current fall time are proportional to commutated current.
- Voltage/current change times are equal in the middle of the semi-sine half-wave at maximal current. This parameter is designated Maximal Duration of Switching (MDS) and for simplicity reasons is equal to 200 ns.
- Drain-to-source on resistance for simplicity reasons is taken equal to 0.1 Ω.
- The analysis is provided for the battery discharge mode only.

Conduction losses of classical MLC with independent sources

For classical MLC with independent sources the sub-module consists of full transistor bridge. In continuous current mode, two switches of each transistor bridge are always conducting semi-sine current. For m-level MLC with independent sources,

$$\Delta P_{FBMLC,c} = m \cdot 2 \cdot \frac{1}{\pi} \int_0^{\pi} \Delta p_c(t) dt = m \cdot 2 \cdot \frac{1}{\pi} \int_0^{\pi} R_{DSon} \cdot (I_{s,m} \cdot \sin\theta)^2 d\theta = \\ = m \cdot 2 \cdot \frac{1}{\pi} \cdot R_{DSon} \cdot I_{s,m}^2 \cdot \frac{1}{2} \pi = m \cdot R_{DSon} \cdot I_{s,m}^2 \ , \tag{4.1}$$

where

$\Delta P_{FBMLC,c}$ – conduction losses of classical MLC with independent sources, W;
m – number of levels;
$\Delta p_c(t)$ – instantaneous conduction losses, W;
R_{Dson} – drain-to-source on-state resistance, Ω;
$I_{s,m}$ – peak value of grid current, A.

Switching losses of classical MLC with independent sources

Speaking about switching losses of MLC with independent sources, it can be said that at each moment of time, one full transistor bridge is working in PWM mode (i.e., two transistors are constantly switching). Switching losses can be calculated by assuming a triangular shape of

instantaneous power on the switches during the commutation. Maximal energy loss of turn-on and turn-off transitions is achieved at grid phase 90° when the current is maximal. For a full-bridge converter,

$$E_{FB,sw,m} = 2 \cdot 2 \cdot \frac{V_{\text{bat}} \cdot I_{s,m} \cdot (t_{i,m} \cdot t_{v,m})}{2} = 2 \cdot V_{\text{bat}} \cdot I_{s,m} \cdot (t_{i,m} \cdot t_{v,m}) = 2 \cdot V_{\text{bat}} \cdot I_{s,m} \cdot MDS \ , \qquad (4.2)$$

where

$E_{FB,sw,m}$ – maximal energy loss for full transistor bridge at 90° phase, J;
V_{bat} – battery voltage, V;
$t_{i,m}$ – maximal current rise/fall time, s;
$t_{v,m}$ – maximal voltage rise/fall time, s;
MDS – Maximal Duration of Switching (previously defined parameter), s.

And maximal power losses are equal to

$$\Delta P_{FB,sw,m} = 2 \cdot V_{\text{bat}} \cdot I_{s,m} \cdot \frac{MDS}{T_{sw}}, \qquad (4.3)$$

where $\Delta P_{FB,sw,m}$ is the maximal power loss for a full transistor bridge at 90° phase, W.

Since the current change times are proportional to the current that is semi-sinusoidal for other points, the equivalent switching losses are calculated as follows:

$$\Delta P_{FB,sw,k} = \frac{1}{T_{sw}} \cdot 2 \cdot 2 \cdot \frac{V_{\text{bat}} \cdot I_{sw,k} \cdot (t_{i,k} \cdot t_{v,k})}{2} = \frac{2}{T_{sw}} \cdot V_{\text{bat}} \cdot I_{s,m} \sin\theta_k \cdot (t_{i,m} \frac{I_{s,k}}{I_{s,m}} + t_v) =$$

$$= \frac{2}{T_{sw}} \cdot V_{\text{bat}} \cdot I_{s,m} \cdot \sin\theta_k \cdot (t_{i,m} \cdot \sin\theta_k + t_v) = \frac{2 \cdot V_{\text{bat}} \cdot I_{s,m} \sin^2\theta_k \cdot \frac{1}{2} MDS}{T_{sw}} + \qquad (4.4)$$

$$+ \frac{2 \cdot V_{\text{bat}} \cdot I_{s,m} \sin\theta_k \cdot \frac{1}{2} MDS}{T_{sw}} = \frac{V_{\text{bat}} \cdot I_{s,m} \cdot MDS}{T_{sw}} \cdot (\sin^2\theta_k + \sin\theta_k) \ ,$$

where

$\Delta P_{FB,sw,k}$ – equivalent power loss for full transistor bridge, W;
T_{sw} – switching period, s;
$I_{sw,k}$ – equivalent commutated current, A;
$t_{i,k}$ – equivalent current rise/fall time, s;
$t_{v,k}$ – equivalent voltage rise/fall time, s;
$I_{s,k}$ – equivalent grid current, A.

Then the total switching losses of classical MLC with independent sources are equal to

$$\Delta P_{FBMLC,sw} = \frac{1}{N} \sum_{k=1}^{N} \Delta P_{FB,sw,k} \ , \qquad (4.5)$$

where N is the number of PWM cycles.

Conduction losses of the multilevel structure of MLC with independent sources and unfolding frontend

Taking into account that in the case of MLC with independent sources and unfolding circuit series-connected multilevel structure consists of half-bridges, in the case of half-bridges, the number of conducting switches for each sub-module is 1. Therefore, taking into consideration (4.1), the conduction losses of series-connected half-bridges in MLC with independent sources and an unfolder are equal to

$$\Delta P_{HBMLC,c} = m \cdot 2 \cdot \frac{1}{\pi} \int_0^{\pi} \Delta p_c(t) dt = \frac{m}{2} \cdot R_{DSon} \cdot I_{s,m}^2, \tag{4.6}$$

where $\Delta P_{HBMLC,c}$ are conduction losses of the multilevel structure of MLC with independent sources and unfolding frontend, W.

Switching losses of the multilevel structure of MLC with independent sources and an unfolding frontend

As it was previously said, for classical MLC with independent sources at each moment of time, one sub-module is working in PWM mode. The same is true for MLC with independent sources, and in the case of half-bridge modules, two transistors are also constantly switching. Switching losses of the multilevel structure of MLC with an unfolding frontend will be the same as in (4.4) and (4.5):

$$\Delta P_{HB,sw,k} = \frac{V_{\text{bat}} \cdot I_{s,m} \cdot MDS}{T_{sw}} \cdot (\sin^2 \theta_k + \sin \theta_k), \tag{4.7}$$

where $\Delta P_{HB,sw,k}$ is the equivalent power loss for the transistor half-bridge, W.

$$\Delta P_{HBMLC,sw} = \frac{1}{N} \sum_{k=1}^{N} \Delta P_{HB,sw,k}, \tag{4.8}$$

where $\Delta P_{HBMLC,sw}$ is the total switching losses of the multilevel structure of MLC with independent sources and unfolding frontend, W.

Losses of the unfolding frontend

In case of unfolding frontend, the grid current in each half-period is constantly flowing through a couple of front-end switches. In this case, the frontend produces only conduction losses, and since switching takes place only every half-period, switching losses can be neglected. This means that

$$\Delta P_{UF,c} = 2 \cdot \frac{1}{\pi} \int_0^{\pi} \Delta p_c(t) dt = 2 \cdot \frac{1}{\pi} \int_0^{\pi} R_{DSon} \cdot (I_{s,m} \cdot \sin \theta)^2 d\theta = R_{DSon} \cdot I_{s,m}^2, \tag{4.9}$$

$$\Delta P_{UF,sw} = 0, \tag{4.10}$$

where $\Delta P_{UF,c}$ – conduction losses of unfolding frontend, W;
$\Delta P_{UF,sw}$ – switching losses of unfolding frontend, W.

The power losses of MLC with independent sources, with and without unfolding circuit, as well as with level modulation, but without pulse modulation, are calculated in a similar way. In this case, switching occurs only two times per half-period. Therefore, the corresponding switching losses can be excluded from the analysis. For m-level MLC,

$$\Delta P_{FBMLC,lm,c} = m \cdot 2 \cdot \frac{1}{\pi} \int_0^{\pi} \Delta p_c(t) dt = m \cdot 2 \cdot \frac{1}{\pi} \int_0^{\pi} R_{DSon} \cdot (I_{s,m} \cdot \sin\theta)^2 d\theta = m \cdot R_{DSon} \cdot I_{s,m}^2 \ , \quad (4.11)$$

$$\Delta P_{HBMLC,lm,c} = m \cdot \frac{1}{\pi} \int_0^{\pi} \Delta p_c(t) dt = m \cdot \frac{1}{\pi} \int_0^{\pi} R_{DSon} \cdot (I_{s,m} \cdot \sin\theta)^2 d\theta = \frac{m}{2} \cdot R_{DSon} \cdot I_{s,m}^2 \ , \quad (4.12)$$

$$\Delta P_{FBMLC,lm,sw} = 0, \quad (4.13)$$

$$\Delta P_{HBMLC,lm,c} = 0, \quad (4.14)$$

where

$\Delta P_{FBMLC,\ lm,c}$ – conduction losses of multilevel structure of MLC with independent sources with level modulation, W;

$\Delta P_{HBMLC,lm,c}$ – conduction losses of multilevel structure of MLC with independent sources and unfolding frontend with level modulation, W;

$\Delta P_{FBMLC,lm,sw}$ – switching losses of classical multilevel structure of MLC with independent sources with level modulation, W;

$\Delta P_{HBMLC,lm,sw}$ – switching losses of multilevel structure of MLC with independent sources and unfolding frontend with level modulation, W.

Evaluation of losses

Power losses of classical MLC with independent sources:

$$\Delta P_{FBMLC} = \Delta P_{FBMLC,c} + \Delta P_{FBMLC,sw} . \quad (4.15)$$

Power losses of MLC with independent sources and unfolding frontend:

$$\Delta P_{HBMLC} = \Delta P_{HBMLC,c} + \Delta P_{HBMLC,sw} + \Delta P_{UF,c} . \quad (4.16)$$

Since the above-described calculation methodology has multiple assumptions, it is irrelevant to demonstrate the actually calculated power losses. However, given that calculation assumptions are the same for all calculation points, for topology comparison, it is reasonable to normalize calculated losses. Calculations were performed for 24 cases – for 3-level, 4-level and 5-level MLC, with unfolding frontend and without it (classical topology). In addition, each topology is combined with 3 + 1 PWM modulation types: with frequencies 2 kHz, 5 kHz and 10 kHz, as well as without PWM modulation (only with level modulation). The resulting losses are normalized with respect to the power losses of a classical 3-level MLC with independent sources. This power loss comparison is shown in Fig. 4.5.

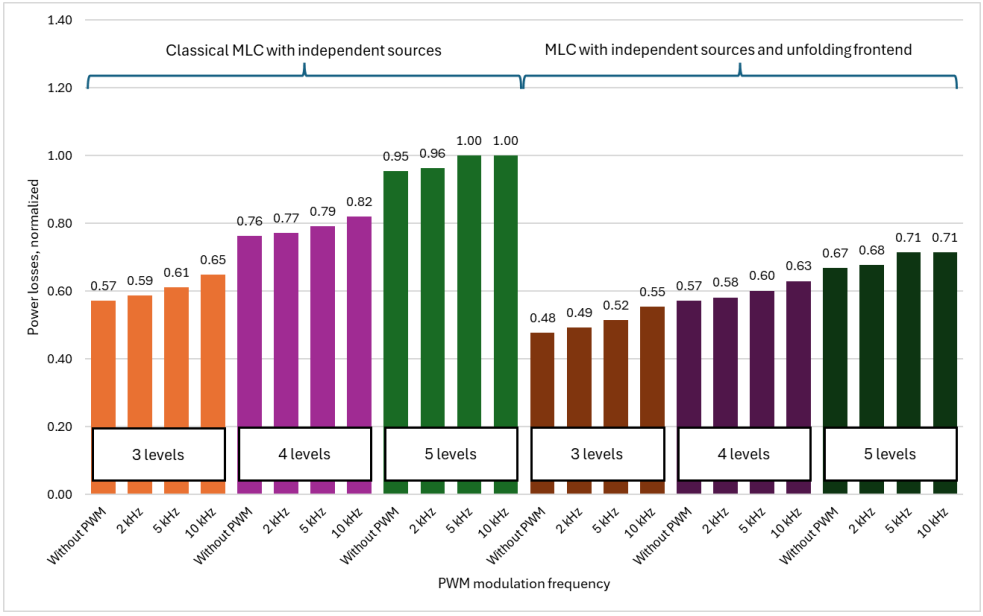

Fig. 4.5. Comparison of power losses of classical MLC with independent sources and MLC with independent sources and unfolding frontend with different level count and different modulation frequencies.

As shown in Fig. 4.5, combining the unfolding frontend with MLC with independent sources gives the ability not only to simplify the topology, but also to reduce overall losses of MLC. With classical MLC with independent sources, when the level count is increased, power losses also noticeably increase. Due to the lower number of transistors in each current path, the change in power losses of MLC with independent sources and unfolder is not so perceivable with an increase in the level count. For example, the power losses of a 3-level MLC with independent sources and an unfolding frontend without PWM are 1.2 times lower. So, the losses are 1.4 times lower in the case of 5-level MLC, unfolding frontend and 10 kHz PWM. Also, it can be seen that switching frequency has a weak impact on the power losses in both cases. Therefore, the conduction losses are the main contributor to the total losses.

4.3. Generalized comparison of topology with fitness function

First of all, a mathematical model for numerical comparison of topologies (classical MLC with independent sources and unfolding MLC with independent sources) has to be brought forward. There is a set of parameters that can be used for the description of these topologies. Some of these parameters are defined by the topology. However, the majority of them are not only defined by the topology but also by the operation mode and working conditions. So, the suitable model is a fitness function with the following parameters:

- Number of switches, S. Number of switches used has an impact on system complexity and cost. For each active switch, there should be a driver circuit, which also affects the overall cost of the converter. The number of switches for m-level single-phase classical MLC with independent sources and unfolding MLC with independent sources can be found as follows:

$$\begin{aligned} S &= 4 \cdot m \text{ – for classical MLC with independent sources;} \\ S &= 2 \cdot m + 4 \text{ – for unfolding MLC with independent sources.} \end{aligned} \tag{4.17}$$

- Redundancy, $1/R$. Redundancy can be represented as the number of possible switching states for voltage levels. Considering that, for example, a full transistor bridge can have $+V_{bat}$, 0 V and $-V_{bat}$, there are three switching states for each level. Redundancy represents control flexibility and, in some cases, fault-tolerant capability of a converter, and for an m-level converter, can be expressed as

$$R = \frac{3^m}{2m+1}. \tag{4.18}$$

- Power losses, ΔP. As it was mentioned in Section 4.2, there are two types of losses – conduction losses and switching losses, which are considered together.
- Harmonic distortion. Harmonic distortion can be divided into two parts: low-frequency harmonic distortion (LFHD) and high-frequency harmonic distortion (HFHD). According to electromagnetic compatibility (EMC) standards (for example, IEC TR 61000-2-5 [73]), frequencies below 9 kHz are considered low. However, for the comparison, frequencies up to the 50th harmonic of the fundamental frequency (2500 Hz for 50 Hz fundamental frequency) will be considered as low-frequency harmonics and frequencies higher than the 50th harmonic – high frequencies. High-frequency harmonics can easily be filtered. Low frequencies are more difficult to filter without corrupting the output waveforms of the converter. With the increase of the level count and PWM modulation frequency, THD will decrease. With PWM modulation, the modulation frequency affects the output voltage. Modulation frequency and frequencies divisible by modulation frequency will have an impact on distortion. For a case without PWM, harmonic distribution is reverse proportional to the number of harmonic, and the impact on LFHD is significant. Within the comparison, cases without PWM are considered with LFHD = 1, when PWM frequency is lower than 2500 Hz, LFHD is set to 0.5 and for other cases to 0. When PWM is not used, HFHD is going to be set to 0; for PWM frequencies in other cases, it will be set to 1.

Fitness function for topology comparison:

$$F = w_1 \cdot S + w_2 \cdot \frac{1}{R} + w_3 \cdot \Delta P + w_4 \cdot LFHD + w_5 \cdot HFHD, \tag{4.19}$$

where w_1, w_2, w_3, w_4, w_5 are weight coefficients for each function parameter.

Depending on weight coefficients, the priorities for the comparison can be set. Since the fitness function is mainly used for optimization, the function is written in such a way that a

lower function value means better and more optimized performance of the converter. If the function is used for optimization, the function value should be minimized:

$$F \to \min . \tag{4.20}$$

In this case, the fitness function is used for topology comparison; therefore, the sum of all weight coefficients is assumed to be equal to 1. Also, for better representation, all parameters were normalized to the maximal values of each parameter. Table 4.1 shows the calculated normalized parameters of the fitness function for 24 cases – 3-level, 4-level, 5-level MLC with independent sources, with unfolding frontend and without it (classical topology). Each case is evaluated with 3 PWM modulation frequencies (2 kHz, 5 kHz and 10 kHz) and without PWM modulation (with level modulation only). Normalized losses were taken from calculations described in Section 4.2.

Table 4.1

Parameters of the Fitness Function

			S (normalized)	$1/R$ (normalized)	ΔP (normalized)	LFHD	HFHD
Classical MLC	3 levels	No PWM	0.6	1.00	0.57	1	0
		2 kHz	0.6	1.00	0.59	0.5	0.5
		5 kHz	0.6	1.00	0.61	0	1
		10 kHz	0.6	1.00	0.65	0	1
	4 levels	No PWM	0.8	0.43	0.76	1	0
		2 kHz	0.8	0.43	0.77	0.5	0.5
		5 kHz	0.8	0.43	0.79	0	1
		10 kHz	0.8	0.43	0.82	0	1
	5 levels	No PWM	1	0.17	0.95	1	0
		2 kHz	1	0.17	0.96	0.5	0.5
		5 kHz	1	0.17	1.00	0	1
		10 kHz	1	0.17	1.00	0	1
MLC with unfolding frontend	3 levels	No PWM	0.5	1.00	0.48	1	0
		2 kHz	0.5	1.00	0.49	0.5	0.5
		5 kHz	0.5	1.00	0.52	0	1
		10 kHz	0.5	1.00	0.55	0	1
	4 levels	No PWM	0.6	0.43	0.57	1	0
		2 kHz	0.6	0.43	0.58	0.5	0.5
		5 kHz	0.6	0.43	0.60	0	1
		10 kHz	0.6	0.43	0.63	0	1
	5 levels	No PWM	0.7	0.17	0.67	1	0
		2 kHz	0.7	0.17	0.68	0.5	0.5
		5 kHz	0.7	0.17	0.71	0	1
		10 kHz	0.7	0.17	0.71	0	1

Figure 4.6 shows the values of the calculated fitness function.

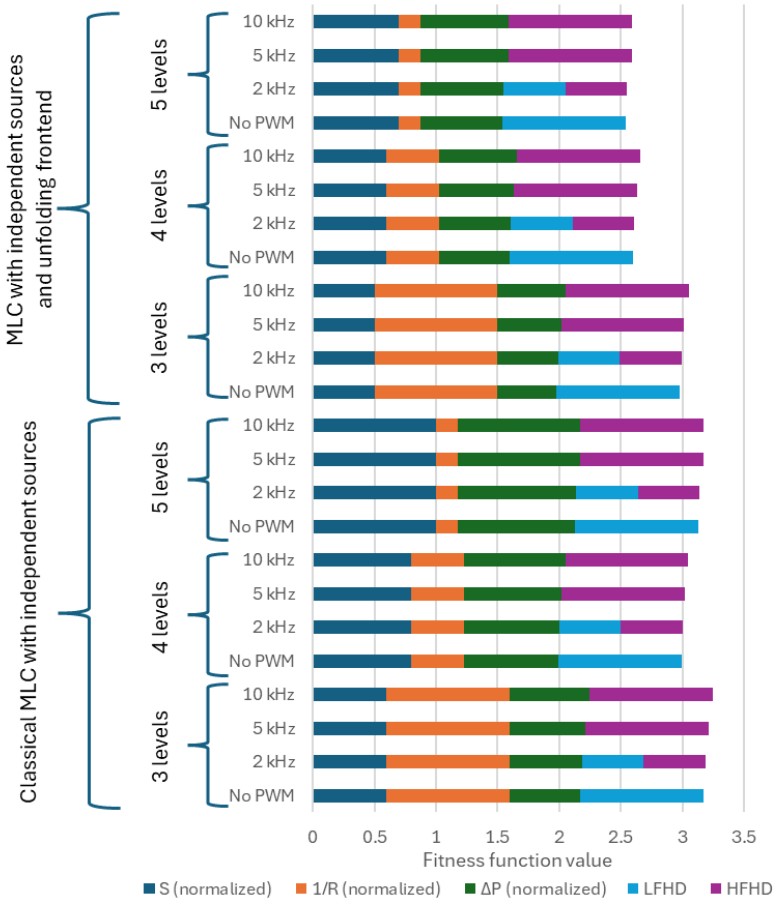

Fig. 4.6. Comparison of classical MLC with independent sources and unfolding MLC with independent sources at different level counts and different modulation frequencies by means of fitness function (lower is better).

Fitness function values, represented in Table 4.1 and Fig. 4.6, show that the overall performance of the MLC with independent sources and unfolding frontend is better than that of the classical MLC with independent sources. Comparing switch count, unfolding MLC with independent sources has 1.2 (for 3-level converter) to 1.43 times (for 5-level converter) lower switch count. The higher level count corresponds to the stronger impact of the unfolding converter. In contrast, the higher level count corresponds to a lower redundancy $1/R$ parameter. As it was previously concluded (Section 4.2), the use of an unfolding converter leads to lower losses of the converter. Regarding LFHD and HFHD, it can be said that PWM frequency should be chosen considering EMC standards and should be higher than the 50th harmonic of the fundamental frequency.

5. MULTILEVEL CONVERTERS WITH INDEPENDENT SOURCES AND HYBRID MODULATION

Author's publications X [74] and V [75], Patent XIII and unpublished publication IV are related to Chapter 5.

5.1. Multilevel converters with hybrid modulation in DC-DC applications

Separate regulation of the current or light flux of individual LED strings (segmented LED light source, SLLS) is associated with a known problem: the necessity of using a controllable LED driver for each string, which increases the total component count, overall system complexity and costs. Therefore, a special multiple-channel LED driving approach (single-inductor multiple-output (SIMO) current source mode (CSM) LED driver) has been chosen to overcome the shortcomings mentioned above. The same multiple-output driving approach can be useful in many other LED applications, such as horticultural lighting, controllable RGB ambient lighting, adjustable correlated color temperature applications, matrix automotive lighting, etc. The approach itself can be considered as a multilevel current and light regulation method with fluent control between levels. The current regulation in the given application is not the primary goal (the primary goal is light regulation), and it is not explicit. However, having an isolating and parallelizing current commutating matrix and combining it with a set of simplified uncontrolled current sources with one controlled current source, it becomes possible to achieve more straightforward and explicit current regulation that widens the range of potential applications. For instance, it enables the use of a similar approach in battery applications – BESSs and chargers for larger or smaller AEVs.

To control individual LED strings, a SIMO CSM driver approach (which by itself can be represented as a multilevel structure) was derived, and a multilevel structure with constant current source (CCS) and light flux regulator (LR) was proposed (shown in Fig. 5.1 (a)). Each LR1 is constructed as a combination (series connection) of a single current regulator CR1 and a chosen number of current switches CS1y, which are controllable switches Q31y connected in parallel with light-emitting diodes LED1y1 … LED1yz, where y is the numbering index for current switches, while z is the numbering index for LEDs. Current regulator CR1 consists of capacitor C21 connected in parallel with LED11 … LED1z, they are connected in series with an uncontrolled switch – diode VD21 (which, in general, can also be a controllable switch). Controllable power switch Q21 is connected in parallel with all these components. Q21 is controlled by a PWM signal. The average current value $I_{LED,CR1}$ of the CR1 branch of light diodes LED11 … LED1z depends on the value of the transistor Q21 control signal duty cycle D_{Q21} and the constant current value I_{L1}, and is equal to

$$I_{LED,CR1} = I_{L1} \cdot (1 - D_{Q21}). \tag{5.1}$$

LR implementation in such a configuration allows the control of light flux with the help of hybrid modulation – one stage is controlled by a PWM signal, the other stages are turned on

and off fully. This, in turn, makes this proposed multilevel structure similar to MLC with independent sources, but in this case, light flux is being controlled.

To optimize the number of controllable switches in LR, it is possible to choose binary-weighted LED numbers in the CSxy branches, where *x* is the numbering index of LRs and CRs (as shown in Fig. 5.1 (a)).

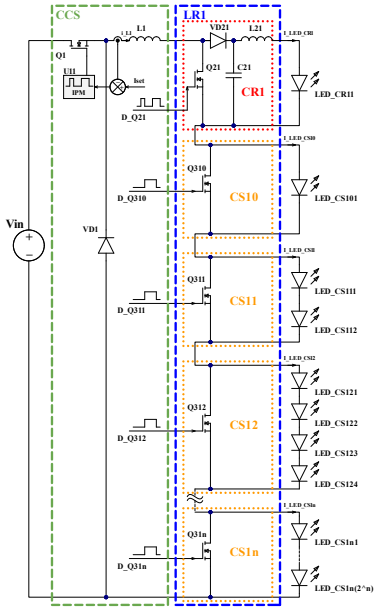

(a)

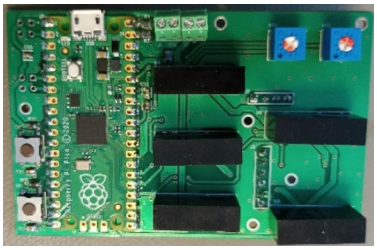

(b)

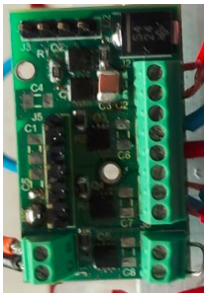

(c)

Fig. 5.1. (a) Implementation of light flux regulator in CSM SIMO LED driver using binary-weighted LEDs; (b) prototype of control and FET driver board; (c) prototype of power part.

For experimental validation, the prototype of the proposed modified SIMO driver was built by combining CCS based on an MP24833 LED driver IC and one LR stage. The LR for testing purposes was built on two separate stackable PCBs/boards, splitting the power part and control part. The LR stage (power part, which is shown in Fig. 5.1 (c)) of the prototype is configured as the combination of one current regulator CR1 with four current switches, CS0 … CS3. For testing purposes, the most robust FET driving circuit configuration was selected for implementation in the prototype board: isolated gate drivers with an isolated supply for each driver. The control system was implemented using an LR RP2040 microcontroller. For testing purposes, two control parameter input methods were implemented: (1) by trimmer and MCU readings of its set value on ADC input; and (2) by “increase”/“decrease” push-buttons. A board of the control parts of the prototype is shown in Fig. 5.1 (b). The testing setup for the experimental validation of the proposed LR is shown in Fig. 5.2. Summaries of the initial tests are given in Figs. 5.3 and 5.4.

The experimental validation of single LR stage luminous flux regulation is shown in Fig. 5.3. The measurements were made with an indirect method using a luxmeter at the central point below the LED module. Correspondence of the control signals to the illuminance at the

center point below the LED module at a distance of 1.1 m is shown there. The tests were conducted with the white, high-power LEDs available in the laboratory: Seoul Semiconductor W724C0 LEDs. The configuration of the module was made as shown in Fig. 5.1 (a), except for the number of CS stages (three stages). The placement of LEDs is close to each other, but not perfectly symmetrical. Thus, the deviation of the experimental points across a linear interpolation is seen in Fig. 5.3, close to the transition points when switching to the next CS combination state.

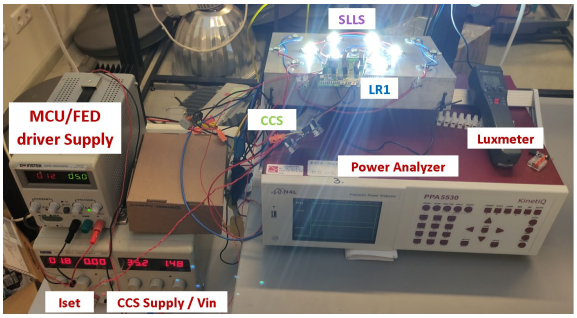

Fig. 5.2. Testing setup for experimental validation.

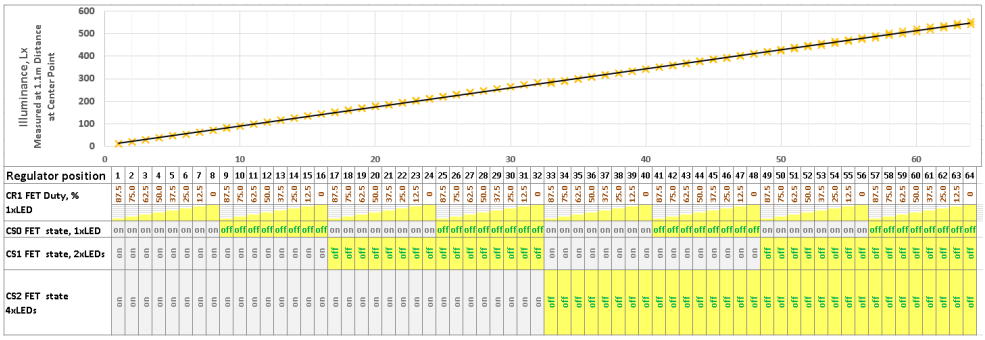

Fig. 5.3. Experimental validation of single LR stage: correspondence of control signals to the illuminance at a center point below the LED module at 1.1 m distance.

The assessment of the efficiency of the proposed system configuration is given in Fig. 5.4. The tests for all dimming options were performed in similar conditions to the LED module mentioned above, with the maximum output power approximately 50 W using eight LEDs in total. Input voltage in all conducted experiments was the same, 35 V. The data obtained using the PPA5530 precision power analyzer were used for this experimental efficiency validation. It is seen here that the efficiency of the bare CCS part is noticeably better in comparison with the combination of CCS + current regulator (CR), which is the price for using such a kind of SIMO driver in high-power applications. However, as can be seen from Fig. 5.4, some efficiency improvements can be achieved using the proposed configuration with light regulator stages.

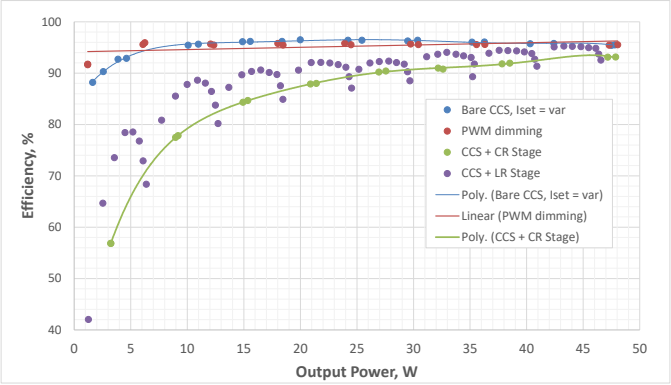

Fig. 5.4. Comparison of the efficiency of different dimmable system configurations by the assessment of experimental data under similar conditions.

5.2. Multilevel converters with independent sources and hybrid modulation in DC-AC applications

As it was mentioned in Chapter 4, application of unfolding frontend together with MLC with independent sources allows for reducing the switch count without losing the advantages of the converter. However, considering applications with batteries and voltage dependence on SOC, as well as the fact that both full transistor bridge and half-bridge are operating only in buck-mode, a number of battery cells connected as MLC inputs should be chosen with respect to fully discharged battery cell voltage, which is not always an option. The other option is to ensure voltage pre-regulation with an additional conversion stage. Such an approach was proposed in [75], where, to the structure of MLC with independent sources and unfolding frontend, the buck-boost stage between the batteries and the half-bridges was added. This allows to regulate the voltage of each module connected in series. The proposed converter structure is shown in Fig. 5.5.

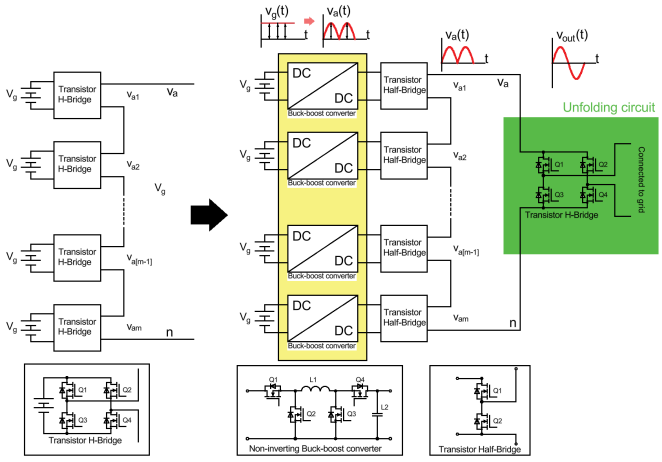

Fig. 5.5. MLC with independent sources, unfolding frontend and pre-regulation stage.

However, considering an additional conversion stage for each series-connected sub-module and a significant increase in switches (which would cause an increase in switching losses), this solution is of no practical interest.

But, in a different configuration, by combining MLC with unfolder and hybrid modulation, described in Section 5.1, it is possible to achieve fluent waveform regulation without losing the advantages of MLC with independent sources. The new configuration of MLC with unfolding frontend and hybrid modulation is shown in Fig. 5.6.

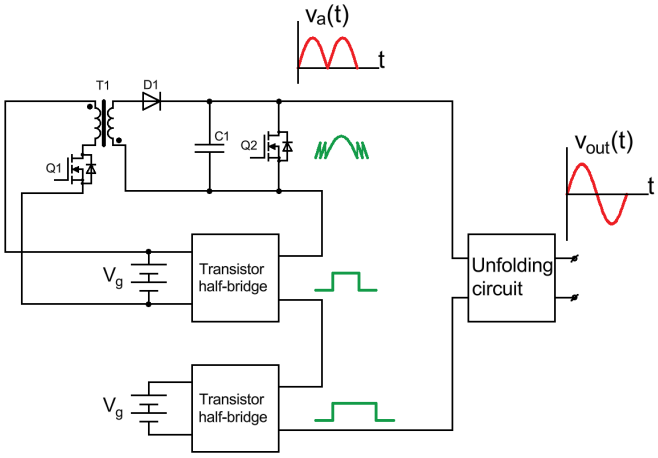

Fig. 5.6. MLC with independent sources, unfolding frontend and hybrid modulation.

As shown in Fig. 5.6, a flyback converter is added to the structure of a two-level MLC with an unfolder. The flyback converter is capable of operating both in buck and boost modes, and by constantly changing duty cycle according to the reference signal, can regulate output waveforms, while series-connected half bridges operate in "on"/"off" mode (without PWM modulation). The operation principles of the flyback are derived from [76]. To ensure bidirectional operation, switch Q2 is added to the schematic. Flyback operation modes are shown in Fig. 5.7.

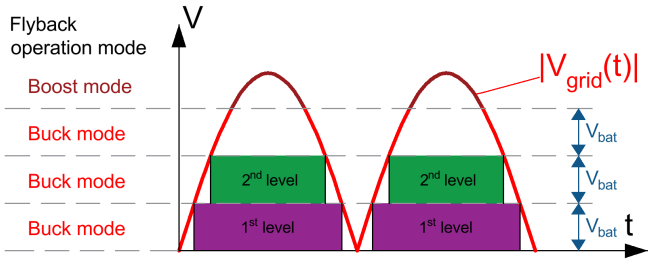

Fig. 5.7. Flyback and half-bridge operation modes.

To evaluate the proposed topology, a *Matlab/Simulink* model was developed (Fig. 5.8). Primary model parameters are shown in Table 5.1.

Table 5.1

Simulation Model Parameters

Parameter	Value
Input voltage	2 batteries, 100 V each
Output voltage	AC 50 Hz, 325 V peak
Load	$R = 20\ \Omega$
Flyback transformer parameters	$L1 = L2 = 4$ µH, coupling coefficient = 0.99
Flyback output capacitor	20 µF
Flyback voltage closed-loop PI controller parameters	$K_P = 0.449$; $K_I = 0.000398$
Flyback switching frequency	100 kHz

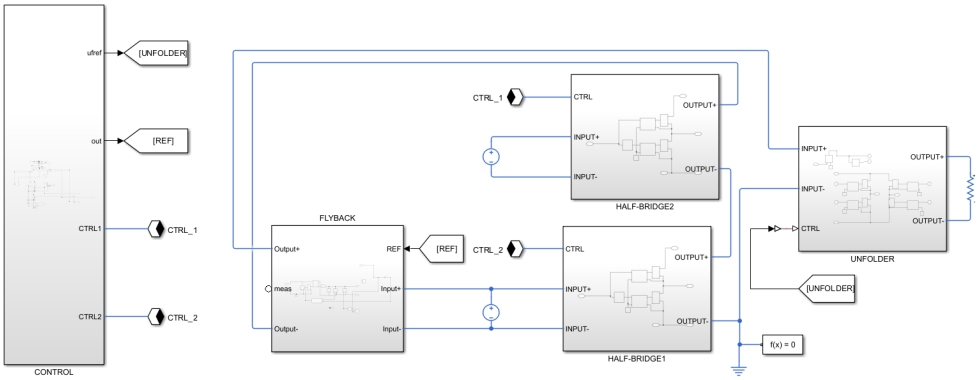

Fig. 5.9. Matlab/Simulink model of proposed MLC configuration.

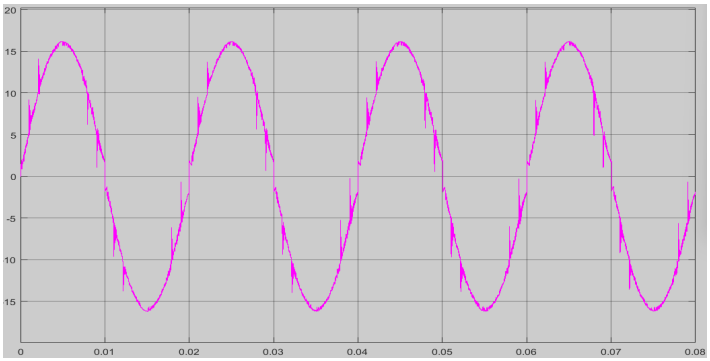

Fig. 5.9. Simulated current waveform of proposed topology.

Shown in Fig. 5.9, the simulated current waveform shows the working capability of the proposed topology. Current spikes are visible on the obtained waveform, which appear during half-bridge module commutation. This can be explained by the insufficient reaction time of the control system (voltage closed-loop control was implemented in the model).

CONCLUSIONS

The study of classical multilevel converter topologies has led to conclusions about the applications of these topologies with batteries, especially multilevel converters with independent sources being more distinguished for that application. This topology has natural battery balancing capability, which is an advantage in applications with batteries.

A novel source balancing method during one period of output voltage for multilevel converters with independent sources was proposed. The method was validated with the help of a simulation model; the results indicate balanced discharge of a three-phase multilevel converter with independent sources.

Several configurations of multilevel converters with independent sources were proposed to enhance the properties of the classical multilevel converter with independent sources topology without losing all the topology advantages.

The impact of the application of the unfolding circuit on power electronic converters was analyzed. Due to low commutation frequency, the unfolding circuit reduces overall switching losses of a converter compared with the pulse-mode frontend. By integrating an unfolding circuit with a multilevel converter with independent sources, it is possible to simplify the multilevel converter topology and reduce the number of switches in the current path. Comparison of classical MLC with independent sources and unfolding MLC with independent sources has been performed with the help of a mathematical model for loss evaluation and with the help of a fitness function. It can be concluded:

- Use of an unfolding frontend enables the opportunity for switch reduction. The effect is more noticeable if the level count is higher. Switch count of unfolding MLC is 1.2 times lower in the case of 3-level converter and 1.43 times lower in the case of 5 levels (compared with classical MLC).
- Lower switch count results in lower overall converter power losses. Power losses are 1.2 times lower in the case of 3-level unfolding MLC with independent sources and 1.4 times lower in the case of 5-level unfolding MLC.
- Higher PWM frequency results in lower low-frequency distortion and higher high-frequency distortion. High-frequency distortion imposes conditions for the output filter. However, high frequencies can be filtered. Low-frequency distortion is difficult to filter without corrupting output waveforms.

With the switch count decrease, the converter losses are also decreased, thereby confirming the proposed hypothesis.

A hybrid modulation method for multilevel converters was proposed and adapted for LED applications. A multilevel structure was developed, which is not a classical multilevel converter with independent sources. However, the operating principles are the same in relation to light flux. After experimental verification of the systems, it can be concluded that although in terms of efficiency the proposed solution is not superior to current source mode dimming driver (reaching up to 94 % maximal efficiency at higher power, with lower efficiency at lower power – starting from 42 % efficiency), in terms of light flux regulation gives the ability of fluent control of light flux.

The same modulation method can be applied to a multilevel converter with independent sources and an unfolding circuit. By adding a flyback converter to the multilevel structure (and the flyback converter input connecting to one of the half-bridge sources), fluent output waveform regulation can be achieved, saving all the multilevel converter advantages. The proposed solution was evaluated using a simulation model, and the results confirm the functionality of the proposed solution; however, some improvements in the control system are required.

Solutions described in this Doctoral Thesis were implemented in four national and international research projects.

REFERENCES

[1] I. A. Galkin, A. Blinov, M. Vorobyov, A. Bubovich, R. Saltanovs, and D. Peftitsis, "Interface Converters for Residential Battery Energy Storage Systems: Practices, Difficulties and Prospects," *Energies 2021,* vol. 14, no. 12, p. 3365, Jun. 2021, doi: 10.3390/EN14123365.

[2] A. Bubovich, M. Vorobyov, I. Galkin, A. Blinov, and A. Giannakis, "Overview of Bidirectional Unfolding Converters for Battery Energy Storage Systems," *2022 IEEE 13th International Symposium on Power Electronics for Distributed Generation Systems, PEDG 2022*, 2022, doi: 10.1109/PEDG54999.2022.9923093.

[3] R. Spotnitz, "Introduction to Batteries | IEEE Courses | IEEE Xplore." Accessed: Sep. 24, 2022. [Online]. Available: https://ieeexplore.ieee.org/courses/details/EDP351

[4] X. Hu, C. Zou, C. Zhang, and Y. Li, "Technological Developments in Batteries: A Survey of Principal Roles, Types, and Management Needs," *IEEE Power and Energy Magazine*, vol. 15, no. 5, pp. 20–31, Sep. 2017, doi: 10.1109/MPE.2017.2708812.

[5] "Electricity storage and renewables: Costs and markets to 2030," 2017. Accessed: Sep. 24, 2022. [Online]. Available: https://www.irena.org/publications/2017/oct/electricity-storage-and-renewables-costs-and-markets

[6] J. Cao and A. Emadi, "Batteries need electronics: Battery management systems vary according to chemistry and applications," *IEEE Industrial Electronics Magazine*, vol. 5, no. 1, pp. 27–35, Mar. 2011, doi: 10.1109/MIE.2011.940251.

[7] B. Ferreira, "Batteries, the New Kids on the Block," *IEEE Power Electronics Magazine*, vol. 6, no. 4, pp. 32–34, Dec. 2019, doi: 10.1109/MPEL.2019.2947980.

[8] C. Chen, S. Plunkett, M. Salameh, S. Stoyanov, S. Al-Hallaj, and M. Krishnamurthy, "Enhancing the Fast Charging Capability of High-Energy-Density Lithium-Ion Batteries: A Pack Design Perspective," *IEEE Electrification Magazine*, vol. 8, no. 3, pp. 62–69, Sep. 2020, doi: 10.1109/MELE.2020.3005700.

[9] "Energy." Accessed: Sep. 24, 2022. [Online]. Available: https://energy.ec.europa.eu/index_en

[10] G. Fulli, M. Masera, A. Spisto, and S. Vitiello, "A change is coming: How regulation and innovation are reshaping the European Union's electricity markets," *IEEE Power and Energy Magazine*, vol. 17, no. 1, pp. 53–66, Jan. 2019, doi: 10.1109/MPE.2018.2872303.

[11] S. M. Lukic and A. Emadi, "Charging ahead," *IEEE Industrial Electronics Magazine*, vol. 2, no. 4, pp. 2–12, 2008, doi: 10.1109/MIE.2008.930361.

[12] A. Khaligh and Z. Li, "Battery, ultracapacitor, fuel cell, and hybrid energy storage systems for electric, hybrid electric, fuel cell, and plug-in hybrid electric vehicles: State of the art," *IEEE Trans. Veh. Technol.*, vol. 59, no. 6, pp. 2806–2814, Jul. 2010, doi: 10.1109/TVT.2010.2047877.

[13] J. Quirós-Tortós, L. Ochoa, and T. Butler, "How electric vehicles and the grid work together: Lessons learned from one of the largest electric vehicle trials in the world,"

IEEE Power and Energy Magazine, vol. 16, no. 6, pp. 64–76, 2018, doi: 10.1109/MPE.2018.2863060.

[14] N. Chen, J. Ma, M. Li, M. Wang, and X. Shen, "Energy management framework for mobile vehicular electric storage," *IEEE Netw.*, vol. 33, no. 6, pp. 148–155, Nov. 2019, doi: 10.1109/MNET.2019.1800546.

[15] S. Chandler, J. Gartner, and D. Jones, "Integrating electric vehicles with energy storage and grids: New technology and specific capabilities spur numerous applications," *IEEE Electrification Magazine*, vol. 6, no. 3, pp. 38–43, Sep. 2018, doi: 10.1109/MELE.2018.2849899.

[16] S. Al-Rubaye, A. Al-Dulaimi, and Q. Ni, "Power Interchange Analysis for Reliable Vehicle-to-Grid Connectivity," *IEEE Communications Magazine*, vol. 57, no. 8, pp. 105–111, Aug. 2019, doi: 10.1109/MCOM.2019.1800657.

[17] P. Arboleya, P. Bidaguren, and U. Armendariz, "Energy is on board: Energy storage and other alternatives in modern light railways," *IEEE Electrification Magazine*, vol. 4, no. 3, pp. 30–41, Sep. 2016, doi: 10.1109/MELE.2016.2584938.

[18] P. Sinhuber, W. Rohlfs, and D. U. Sauer, "Study on power and energy demand for sizing the energy storage systems for electrified local public transport buses," *2012 IEEE Vehicle Power and Propulsion Conference, VPPC 2012*, pp. 315–320, Jan. 2012, doi: 10.1109/VPPC.2012.6422680.

[19] M. Guarnieri, M. Morandin, A. Ferrari, P. Campostrini, and S. Bolognani, "Electrifying water buses," *IEEE Industry Applications Magazine*, vol. 24, no. 1, pp. 71–83, Jan. 2018, doi: 10.1109/MIAS.2017.2739998.

[20] A. J. Sorensen *et al.*, "Toward Safer, Smarter, and Greener Ships: Using Hybrid Marine Power Plants," *IEEE Electrification Magazine*, vol. 5, no. 3, pp. 68–73, Sep. 2017, doi: 10.1109/MELE.2017.2718861.

[21] D. Paul, "A History of Electric Ship Propulsion Systems [History]," *IEEE Industry Applications Magazine*, vol. 26, no. 6, pp. 9–19, Nov. 2020, doi: 10.1109/MIAS.2020.3014837.

[22] A. Vicenzutti, D. Bosich, G. Giadrossi, and G. Sulligoi, "The Role of Voltage Controls in Modern All-Electric Ships: Toward the all-electric ship," *IEEE Electrification Magazine*, vol. 3, no. 2, pp. 49–65, Jun. 2015, doi: 10.1109/MELE.2015.2413437.

[23] M. Stecca, L. R. Elizondo, T. B. Soeiro, P. Bauer, and P. Palensky, "A comprehensive review of the integration of battery energy storage systems into distribution networks," *IEEE Open Journal of the Industrial Electronics Society*, vol. 1, no. 1, pp. 46–65, 2020, doi: 10.1109/OJIES.2020.2981832.

[24] D. Manz, R. Piwko, and N. Miller, "Look before you leap: The role of energy storage in the grid," *IEEE Power and Energy Magazine*, vol. 10, no. 4, pp. 75–84, 2012, doi: 10.1109/MPE.2012.2196337.

[25] M. Farrokhabadi *et al.*, "Energy Storage in Microgrids: Compensating for Generation and Demand Fluctuations while Providing Ancillary Services," *IEEE Power and Energy Magazine*, vol. 15, no. 5, pp. 81–91, Sep. 2017, doi: 10.1109/MPE.2017.2708863.

[26] A. Cagnano, E. de Tuglie, and P. Mancarella, “Microgrids: Overview and guidelines for practical implementations and operation,” *Appl Energy*, vol. 258, p. 114039, Jan. 2020, doi: 10.1016/J.APENERGY.2019.114039.

[27] J. L. Torres-Moreno, A. Gimenez-Fernandez, M. Perez-Garcia, and F. Rodriguez, “Energy Management Strategy for Micro-Grids with PV-Battery Systems and Electric Vehicles,” *Energies 2018,* vol. 11, no. 3, p. 522, Feb. 2018, doi: 10.3390/EN11030522.

[28] P. Lezynski, P. Szczesniak, B. Waskowicz, R. Smolenski, and W. Drozdz, “Design and Implementation of a Fully Controllable Cyber-Physical System for Testing Energy Storage Systems,” *IEEE Access*, vol. 7, pp. 47259–47272, 2019, doi: 10.1109/ACCESS.2019.2907612.

[29] Z. Ma, A. Pesaran, V. Gevorgian, D. Gwinner, and W. Kramer, “Energy Storage, Renewable Power Generation, and the Grid: NREL Capabilities Help to Develop and Test Energy-Storage Technologies,” *IEEE Electrification Magazine*, vol. 3, no. 3, pp. 30–40, Sep. 2015, doi: 10.1109/MELE.2015.2447972.

[30] E. Rodriguez-Diaz, F. Chen, J. C. Vasquez, J. M. Guerrero, R. Burgos, and D. Boroyevich, “Voltage-Level Selection of Future Two-Level LVdc Distribution Grids: A Compromise between Grid Compatibility, Safety, and Efficiency,” *IEEE Electrification Magazine*, vol. 4, no. 2, pp. 20–28, Jun. 2016, doi: 10.1109/MELE.2016.2543979.

[31] A. Bubovich, M. Vorobyov, A. Blinov, and D. Peftitsis, “Peculiarities of Multilevel Power Electronic Converters for Interfacing Battery Energy Storages with AC Loads,” *2020 IEEE 8th Workshop on Advances in Information, Electronic and Electrical Engineering, AIEEE 2020 – Proceedings*, Apr. 2021, doi: 10.1109/AIEEE51419.2021.9435798.

[32] A. Bubovich and I. Galkin, “Evaluation of Optimal Switching of Modular Multilevel Inverter with Independent Voltage Sources,” in *2020 IEEE 61st Annual International Scientific Conference on Power and Electrical Engineering of Riga Technical University, RTUCON 2020 – Proceedings*, Institute of Electrical and Electronics Engineers Inc., Nov. 2020. doi: 10.1109/RTUCON51174.2020.9316581.

[33] I. Colak, E. Kabalci, and R. Bayindir, “Review of multilevel voltage source inverter topologies and control schemes,” *Energy Convers Manag*, vol. 52, no. 2, pp. 1114–1128, Feb. 2011, doi: 10.1016/j.enconman.2010.09.006.

[34] A. Nabae, I. Takahashi, and H. Akagi, “A New Neutral-Point-Clamped PWM Inverter,” *IEEE Trans Ind Appl*, vol. IA-17, no. 5, pp. 518–523, 1981, doi: 10.1109/TIA.1981.4503992.

[35] S. Khomfoi and L. M. Tolbert, “Multilevel Power Converters,” in *Power Electronics Handbook*, 2nd ed., Elsevier Inc., 2006, ch. 17, pp. 451–482. [Online]. Available: http://web.eecs.utk.edu/~tolbert/publications/multilevel_book_chapter.pdf

[36] M. Moradpour, P. Ghani, P. Pirino, and G. Gatto, “A GaN-Based Battery Energy Storage System for Three-Phase Residential Application with Series-Stacked Devices and Three-Level Neutral Point Clamped Topology,” in *SyNERGY MED 2019 - 1st International Conference on Energy Transition in the Mediterranean Area*, Institute of Electrical and Electronics Engineers Inc., May 2019. doi: 10.1109/SyNERGY-MED.2019.8764117.

[37] U. Abronzini *et al.*, “A Dual-Source DHB-NPC Power Converter for Grid Connected Split Battery Energy Storage System,” in *2018 IEEE Energy Conversion Congress and Exposition, ECCE 2018*, Institute of Electrical and Electronics Engineers Inc., Dec. 2018, pp. 2483–2488. doi: 10.1109/ECCE.2018.8557563.

[38] I. Trintis, S. Munk-Nielsen, and R. Teodorescu, “Single stage grid converters for battery energy storage,” in *IET Conference Publications*, 2010. doi: 10.1049/cp.2010.0016.

[39] T. A. Meynard and H. Foch, “Multi-level conversion: High voltage choppers and voltage-source inverters,” in *PESC Record – IEEE Annual Power Electronics Specialists Conference*, Institute of Electrical and Electronics Engineers Inc., 1992, pp. 397–403. doi: 10.1109/PESC.1992.254717.

[40] J. S. Lai and F. Z. Peng, “Multilevel converters – a new breed of power converters,” in *Conference Record – IAS Annual Meeting (IEEE Industry Applications Society)*, IEEE, 1995, pp. 2348–2356. doi: 10.1109/ias.1995.530601.

[41] J. Asakura and H. Akagi, “State-of-Charge (SOC)-Balancing Control of a Battery Energy Storage System Based on a Cascade PWM Converter,” *IEEE Trans Power Electron*, vol. 24, no. 6, pp. 1628–1636, 2009, doi: 10.1109/TPEL.2009.2014868.

[42] I. A. Galkin, R. Saltanovs, A. Bubovich, A. Blinov, and D. Peftitsis, “Considerations on Combining Unfolding Inverters with Partial Power Regulators in Battery-Grid Interface Converters,” *Energies 2024,* vol. 17, no. 4, p. 893, Feb. 2024, doi: 10.3390/EN17040893.

[43] O. Matiushkin, O. Husev, R. Strzelecki, S. Ivanets, and A. Fesenko, “Novel single-stage buck-boost inverter with unfolding circuit,” in *2017 IEEE First Ukraine Conference on Electrical and Computer Engineering (UKRCON)*, IEEE, May 2017, pp. 538–543. doi: 10.1109/UKRCON.2017.8100298.

[44] O. Husev, O. Matiushkin, C. Roncero-Clemente, F. Blaabjerg, and D. Vinnikov, “Novel Family of Single-Stage Buck-Boost Inverters Based on Unfolding Circuit,” *IEEE Trans Power Electron*, vol. 34, no. 8, pp. 7662–7676, 2019, doi: 10.1109/TPEL.2018.2879776.

[45] O. Matiushkin, O. Husev, C. Roncero-Clemente, S. Ivanets, and A. Fesenko, “Component design guidelines for new single-stage buck-boost inverter with unfolding circuit,” *2017 IEEE International Young Scientists Forum on Applied Physics and Engineering, YSF 2017*, vol. 2017-January, pp. 40–45, Dec. 2017, doi: 10.1109/YSF.2017.8126589.

[46] O. Matiushkin, O. Husev, D. Vinnikov, and C. Roncero-Clemente, “Model predictive control for buck-boost inverter based on unfolding circuit,” *2019 IEEE 2nd Ukraine Conference on Electrical and Computer Engineering, UKRCON 2019 – Proceedings*, pp. 431–436, Jul. 2019, doi: 10.1109/UKRCON.2019.8879870.

[47] R. W. Erickson and A. P. Rogers, “A microinverter for building-integrated photovoltaics,” *Conference Proceedings - IEEE Applied Power Electronics Conference and Exposition – APEC*, pp. 911–917, 2009, doi: 10.1109/APEC.2009.4802771.

[48] C. H. Chang and K. H. Ho, “A Transformer-Less High-Gain Inverter with Step-Up/Down and Single Energy-Processing Features,” *IEEE J. Emerg. Sel. Top. Power Electron.*, vol. 9, no. 4, pp. 4726–4738, Aug. 2021, doi: 10.1109/JESTPE.2020.3023107.

[49] W. Wu, J. Ji, and F. Blaabjerg, “Aalborg inverter – A new type of ‘buck in buck, boost in boost’ grid-tied inverter,” *IEEE Trans. Power Electron.*, vol. 30, no. 9, pp. 4784–4793, Sep. 2015, doi: 10.1109/TPEL.2014.2363566.

[50] S. Zhang, W. Wu, H. Wang, M. Huang, N. Gao, and F. Blaabjerg, “Single-stage MPPT control realization for Aalborg inverter in photovoltaic system,” *Proceedings IECON 2017 – 43rd Annual Conference of the IEEE Industrial Electronics Society*, vol. 2017-January, pp. 4233–4238, Dec. 2017, doi: 10.1109/IECON.2017.8216726.

[51] W. Wu, Z. Wang, J. Ji, and F. Blaabjerg, “Performance analysis of new type grid-tied inverter – Aalborg Inverter,” *2014 16th European Conference on Power Electronics and Applications, EPE-ECCE Europe 2014*, 2014, doi: 10.1109/EPE.2014.6910861.

[52] A. Diab-Marzouk and O. Trescases, “SiC-Based Bidirectional ĆUK Converter with Differential Power Processing and MPPT for a Solar Powered Aircraft,” *IEEE Transactions on Transportation Electrification*, vol. 1, no. 4, pp. 369–381, Dec. 2015, doi: 10.1109/TTE.2015.2505302.

[53] D. Bortis, D. Neumayr, and J. W. Kolar, “ηρ-Pareto optimization and comparative evaluation of inverter concepts considered for the GOOGLE Little Box Challenge,” *2016 IEEE 17th Workshop on Control and Modeling for Power Electronics, COMPEL 2016*, 2016, doi: 10.1109/COMPEL.2016.7556767.

[54] J. Everts, F. Krismer, J. Van Den Keybus, J. Driesen, and J. W. Kolar, “Optimal zvs modulation of single-phase single-stage bidirectional dab ac-dc converters,” *IEEE Trans Power Electron*, vol. 29, no. 8, pp. 3954–3970, 2014, doi: 10.1109/TPEL.2013.2292026.

[55] J. Everts, F. Krismer, J. Van Den Keybus, J. Driesen, and J. W. Kolar, “Comparative evaluation of soft-switching, bidirectional, isolated AC/DC converter topologies,” *Conference Proceedings – IEEE Applied Power Electronics Conference and Exposition – APEC*, pp. 1067–1074, 2012, doi: 10.1109/APEC.2012.6165951.

[56] L. Xue, Z. Shen, D. Boroyevich, P. Mattavelli, and D. Diaz, “Dual Active Bridge-Based Battery Charger for Plug-in Hybrid Electric Vehicle with Charging Current Containing Low Frequency Ripple,” *IEEE Trans. Power Electron.*, vol. 30, no. 12, pp. 7299–7307, Dec. 2015, doi: 10.1109/TPEL.2015.2413815.

[57] H. S. Kim, M. H. Ryu, J. W. Baek, and J. H. Jung, “High-efficiency isolated bidirectional AC-DC converter for a DC distribution system,” *IEEE Trans. Power Electron.*, vol. 28, no. 4, pp. 1642–1654, Apr. 2013, doi: 10.1109/TPEL.2012.2213347.

[58] A. Tong, L. Hang, G. Li, X. Jiang, and S. Gao, “Modeling and Analysis of a Dual-Active-Bridge-Isolated Bidirectional DC/DC Converter to Minimize RMS Current with Whole Operating Range,” *IEEE Trans. Power Electron.*, vol. 33, no. 6, pp. 5302–5316, Jun. 2018, doi: 10.1109/TPEL.2017.2692276.

[59] W. Choi, K. M. Rho, and B. H. Cho, “Fundamental Duty Modulation of Dual-Active-Bridge Converter for Wide-Range Operation,” *IEEE Trans. Power Electron.*, vol. 31, no. 6, pp. 4048–4064, Jun. 2016, doi: 10.1109/TPEL.2015.2474135.

[60] J. Hiltunen, V. Vaisanen, R. Juntunen, and P. Silventoinen, “Variable-Frequency Phase Shift Modulation of a Dual Active Bridge Converter,” *IEEE Trans. Power Electron.*, vol. 30, no. 12, pp. 7138–7148, Dec. 2015, doi: 10.1109/TPEL.2015.2390913.

[61] N. Hou and Y. W. Li, "Overview and Comparison of Modulation and Control Strategies for a Nonresonant Single-Phase Dual-Active-Bridge DC-DC Converter," *IEEE Trans. Power Electron.*, vol. 35, no. 3, pp. 3148–3172, Mar. 2020, doi: 10.1109/TPEL.2019.2927930.

[62] Y. Shen, X. Sun, W. Li, X. Wu, and B. Wang, "A Modified Dual Active Bridge Converter with Hybrid Phase-Shift Control for Wide Input Voltage Range," *IEEE Trans. Power Electron.*, vol. 31, no. 10, pp. 6884–6900, Oct. 2016, doi: 10.1109/TPEL.2015.2510033.

[63] D. Sha, X. Wang, and D. Chen, "High-Efficiency Current-Fed Dual Active Bridge DC-DC Converter With ZVS Achievement Throughout Full Range of Load Using Optimized Switching Patterns," *IEEE Trans. Power Electron.*, vol. 33, no. 2, pp. 1347–1357, Feb. 2018, doi: 10.1109/TPEL.2017.2675945.

[64] M. H. Kheraluwala, R. W. Gascoigne, D. M. Divan, and E. D. Baumann, "Performance Characterization of a High-Power Dual Active Bridge dc-to-dc Converter," *IEEE Trans. Ind. Appl.*, vol. 28, no. 6, pp. 1294–1301, 1992, doi: 10.1109/28.175280.

[65] S. A. Q. Mohammed and J. W. Jung, "A State-of-the-Art Review on Soft-Switching Techniques for DC-DC, DC-AC, AC-DC, and AC-AC Power Converters," *IEEE Trans. Industr. Inform.*, vol. 17, no. 10, pp. 6569–6582, Oct. 2021, doi: 10.1109/TII.2021.3058218.

[66] "Design Guide: TIDA-010054 Bidirectional, Dual Active Bridge Reference Design for Level 3 Electric Vehicle Charging Stations," 2021.

[67] A. K. Jain and R. Ayyanar, "PWM control of dual active bridge: Comprehensive analysis and experimental verification," *IEEE Trans. Power Electron.*, vol. 26, no. 4, pp. 1215–1227, 2011, doi: 10.1109/TPEL.2010.2070519.

[68] D. Wang, W. Zhang, and J. Li, "A PWM plus phase shift control strategy for dual-active-bridge DC-DC converter in electric vehicle charging/discharging system," *IEEE Transportation Electrification Conference and Expo, ITEC Asia-Pacific 2014 – Conference Proceedings*, Oct. 2014, doi: 10.1109/ITEC-AP.2014.6940986.

[69] Z. Pavlović, J. A. Oliver, P. Alou, Ó. Garcia, and J. A. Cobos, "Bidirectional dual active bridge series resonant converter with pulse modulation," *Conference Proceedings – IEEE Applied Power Electronics Conference and Exposition – APEC*, pp. 503–508, 2012, doi: 10.1109/APEC.2012.6165867.

[70] H. Wu, K. Sun, Y. Li, and Y. Xing, "Fixed-Frequency PWM-Controlled Bidirectional Current-Fed Soft-Switching Series-Resonant Converter for Energy Storage Applications," *IEEE Transactions on Industrial Electronics*, vol. 64, no. 8, pp. 6190–6201, Aug. 2017, doi: 10.1109/TIE.2017.2682020.

[71] A. Bubovich, M. Vorobyov, and A. Giannakis, "Initial Evaluation of a Multilevel Inverter with Unfolding Stage for BESS Applications," *Proceedings of the 9th IEEE Workshop on Advances in Information, Electronic and Electrical Engineering, AIEEE 2021*, 2021, doi: 10.1109/AIEEE54188.2021.9670386.

[72] H. Akagi, “Classification, terminology, and application of the modular multilevel cascade converter (MMCC),” *IEEE Trans. Power Electron.*, vol. 26, no. 11, pp. 3119–3130, 2011, doi: 10.1109/TPEL.2011.2143431.

[73] INTERNATIONAL ELECTROTECHNICAL COMMISSION, “IEC TR 61000-2-5 – Electromagnetic compatibility (EMC) – Part 2–5: Environment – Description and classification of electromagnetic environments.”

[74] O. Tetervenoks, I. Galkin, and A. Bubovich, “Considerations on Practical Implementation of Current Source Mode Single-Inductor Multiple-Output LED Driver,” *Electronics 2024,* vol. 13, no. 1, p. 54, Dec. 2023, doi: 10.3390/ELECTRONICS13010054.

[75] A. Bubovich, V. Parinova, I. Galkin, and A. Giannakis, “Initial Evaluation of Multilevel Converter with Unfolding Stage and Voltage Regulators for applications in BESSs,” *Proceedings of the Biennial Baltic Electronics Conference, BEC*, vol. 2022-October, 2022, doi: 10.1109/BEC56180.2022.9935611.

[76] Z. Zhao, J. S. Lai, and Y. Cho, “Dual-mode double-carrier-based sinusoidal pulse width modulation inverter with adaptive smooth transition control between modes,” *IEEE Transactions on Industrial Electronics*, vol. 60, no. 5, pp. 2094–2103, 2013, doi: 10.1109/TIE.2012.2227900.

Aleksandrs Bubovičs was born in 1993 in Riga. He received a Bachelor's degree (2017) and a Master's degree (2018) in Computerised Control of Electrical Technologies from Riga Technical University. Since 2016, he has worked at Riga Technical University, where he is currently a researcher, lecturer and laboratory chief. His research interests include the application of power electronic converters in energy storage systems and medical equipment, as well as thermal management of power electronics.